Summer 2015

Synthesis and Functionalization of Fluorescent Quantum Dot Bioconjugates for Cellular Imaging of Directed Gene Therapy

Jason Matthew Davis

SYNTHESIS AND FUNCTIONALIZATION OF FLUORESCENT QUANTUM DOT BIOCONJUGATES FOR CELLULAR IMAGING OF DIRECTED GENE THERAPY

A Masters Thesis

Presented to

The Graduate College of

Missouri State University

In Partial Fulfillment

Of the Requirements for the Degree

Master of Science, Chemistry

By

Jason M. Davis

July 2015

SYNTHESIS AND FUNCTIONALIZATION OF FLUORESCENT QUANTUM DOT BIOCONJUGATES FOR CELLULAR IMAGING OF DIRECTED GENE THERAPY

Chemistry

Missouri State University, July 2015

Masters of Science

Jason M. Davis

ABSTRACT

Herein, I optimize a method for synthesis and bioconjugation of water-soluble, fluorescent CdSe/ZnS quantum dots (QDs) for targeted cellular delivery of DNA. Core CdSe QDs were synthesized in high temperature organic solvents and passivated with a ZnS shell to increase quantum yield. The fluorescent QD nanoparticles were made water-soluble by enveloping them with an amphiphilic polymer. These aqueous nanoparticles were functionalized with tertiary amines to impart a positive charge, allowing electrostatic binding to negatively-charged DNA. The conjugated QDs were characterized using zeta potential and electrophoresis to gauge their ability to electrostatically bind DNA. The QDs were further modified by conjugation with Wheat Germ Agglutinin (WGA) (a carbohydrate-binding protein) in an aim to direct nanoparticle trafficking within the cell. I observed the effect of this conjugation to QDs in N2a (mouse neuroblastoma) cells using fluorescence microscopy and immunocytochemistry to visualize trafficking. The images were used to evaluate the potential of bioconjugated QDs as a targeted non-viral gene therapy vector.

KEYWORDS: quantum dots, gene therapy, nanoparticles, bioconjugation, fluorescence microscopy

This abstract is approved as to form and content

_____

Katye M. Fichter, PhD
Chairperson, Advisory Committee
Missouri State University

SYNTHESIS AND FUNCTIONALIZATION OF FLUORESCENT QUANTUM DOT BIOCONJUGATES FOR CELLULAR IMAGING OF DIRECTED GENE THERAPY

By

Jason M Davis

A Masters Thesis
Submitted to the Graduate College
Of Missouri State University
In Partial Fulfillment of the Requirements
For the Degree of Master of Science, Chemistry

July 2015

Approved: _____
Katye M. Fichter, PhD

_____
Gary Meints, PhD

_____
Reza Herati, PhD

_____
Paul Schweiger, PhD

_____
Julie Masterson, PhD: Dean, Graduate College

ACKNOWLEDGEMENTS

I would like to thank the following people for their support during the course of my graduate studies. Dr. Katye Fichter, my major advisor, for constant help and guidance that would be impossible to ever fully put into words. There were many times throughout that I would have given up without her help and skill. Dr. Gary Meints, whos mentoring in my undergraduate degree encouraged me to go on for a graduate degree in the first place. Dr. Paul Schweiger, who mentored my work with many biological samples I was before unfamiliar with. Dr. Collin Heyes for his input on QD coatings. Dr. Lazlo Kovacs for use of his microscope camera for our early pictures of our QDs. Dr. Reza Herati for his technical support when we first attempted to make polymers. Matt Ellis and Nick Mundt for helping me with countless experimental trials as undergraduates, and even more luck to them as they continue on in their graduate studies. Finally I would like to thank Kalie Somerville, Eric Tague, Jenn Schott, and Aaron Proctor, my closest friends for their support and efforts to keep me in the program until the very end. There are many others who deserve this thanks just as much, but this degree and this work would not have been possible without the help of each and every person I have come into contact with here at Missouri State. Thanks to all of you.

TABLE OF CONTENTS

LIST OF FIGURES

CHAPTER 1: INTRODUCTION

1.1 What are Quantum Dots?

Quantum Dots (QDs) are semiconductor nanocrystals made of group II and IV (*e.g.* cadmium and selenium) or group III and V (*e.g.* indium and phosphorus) elements [1] .The attraction of these nanoparticles is their unique ability to fluoresce in various controllable colors based on their size, as well as superior photostability. Recent advances have looked into surface modification of these QDs for various applications in biomedical research, diagnostics, therapeutics, batteries, solar cells, and many other areas [2, 3]. The ability to tailor QD functionality, along with their increased resistance to photobleaching compared to traditional organic dye, make them a very attractive alternative in biological applications. QDs have an intense fluorescence and a distinctive blinking pattern that can allow for single molecule imaging and tracking within a cell [4]. The key to these superior characteristics lies in the core structure of the quantum dot.

The fluorescent characteristics of QDs that make them unique stems from their size. Typical CdSe QDs range in size from ~2 to 5 nm depending on the fluorescence emission color desired. At this size, the QD exhibits a physical size that is smaller than the exciton Bohr radius. The Bohr radius is the spatial distance between an electron and the hole left behind after excitation [5]. The difference between the Bohr radius of the QD and physical size results in a quantum confinement effect. That is, electrons exist in discrete energy levels instead of continuous energy levels of bulk materials. This confinement causes the smallest band gap to increase in energy as the particle decreases in size, resulting in the emission of higher energy photons [1]. The energy of emitted

photons determines the fluorescence emission color (*i.e.* wavelength). The wavelength of fluorescence emission directly relates to QD size. A red shift occurs as QD size increases and band gap decreases (Figure 1.1).

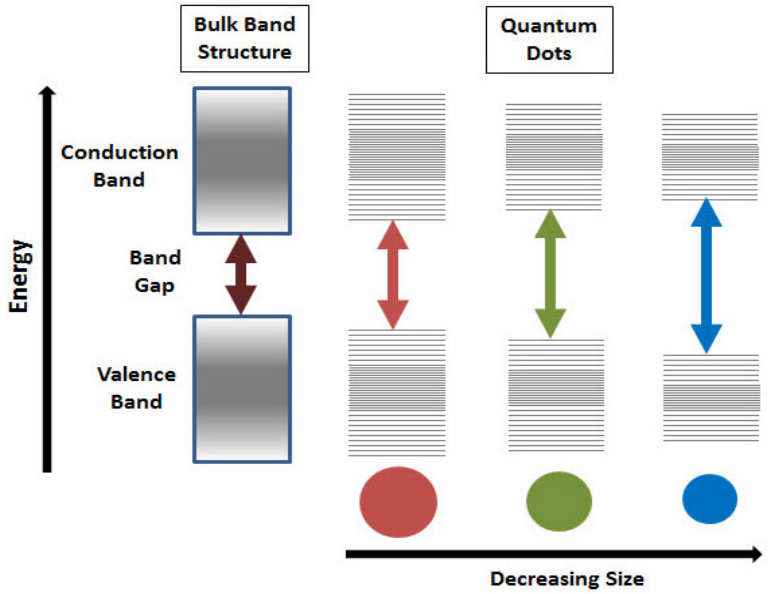

Figure 1.1. The Energy Relationship Between QD Size and Fluorescence Emission Color [6]. QD size is directly proportional to wavelength of the emitted photon. Quantum confinement results in discrete energy levels. The difference between the two energy levels (i.e. valence and conduction bands) increases as QD size decreases. This increase in band gap energy decreases the wavelength of the emitted photon, appearing as a blue-shift in fluorescence emission.

The small size of QDs allows for delocalization of the electrons around the nanocrystal. When electrons are irradiated with UV light an exciton pair is generated. An exciton pair is an excited electron and the partially positive "hole" left behind. Under normal circumstances an electron will recombine with the hole, which results in an emission of a photon. This is called radiative relaxation. If an excited electron is free to move around the nanocrystals, it can relax through non-radiative processes. Non-radiative processes include vibrational and rotational energy modes that relax an electron without

the release of a photon. If an electron relaxes through non-radiative processes, it may no longer recombine with the hole, causing a surface defect, or a trap state. Trap states effectively decrease the fluorescence and quantum yield of QDs. While trap states are detrimental to the quality of the core, there are methods to help prevent loss of fluorescence [7]. The main method is addition of a coating onto the outside of the core to help prevent surface defects. The addition of a coating results in what is called a core-shell system (Figure 1.3). Coating QDs requires careful characterization of the cores to optimize core-shell quality.

Core quality can be quickly determined through the use of fluorescence spectra. Fluorescence spectra can indicate the size distribution of QDs in solution. The peak width in a fluorescence spectrum is indicative of the QD size distribution. A typical synthesis of high-quality CdSe QDs has a fluorescence emission peak with a full width at half maximum (FWHM) range of 25 +/- 2 nm [8]. The typical width in this work was 26-30 nm.

The narrow size distribution of these QDs is obtained by carefully controlling reactants and limiting nucleation and growth times. While large (~5-6 nm) QDs are easier to synthesize than small QDs, creating large-sized QDs with a narrow size distribution is challenging due to Ostwald's ripening. Ostwald ripening is a thermodynamically driven process by which smaller particles dissolve and deposit onto larger particles, effectively widening the size distribution of nanoparticles [9]. When the concentration of a precursor falls below nucleation levels, Ostwald's ripening can occur during QD synthesis. Smaller nucleated crystals dissolve and larger crystals grow resulting in a wider size distribution. This is evident in the FWHM of a fluorescence spectrum. To control Ostwald's ripening, precursor solutions and reaction times are meticulously monitored during synthesis. This

minimizes the size distribution, which allows for more accurate calculation of QD concentration and diameter.

The diameter, in nanometers, of a given solution of CdSe particles can be calculated with the first exciton absorption peak (λ) in nm. This equation is derived from experimental data provided by W. W. Yu et al [8] and covers a range of excitation peaks λ from 300 to 700 nm. For our synthesis, the first excitonic peak typically fell between 630-650 nm; therefore, this equation is applicable to our QD products. The equation uses the first exciton absorption peak (λ in nm) and can be seen here:

$$D = (1.6122x10^{-9})\lambda^4 - (2.6575x10^{-6})\lambda^3 + (1.6242x10^{-3})\lambda^2 - (0.4277)\lambda + 41.57$$

Once the diameter is calculated, the extinction coefficient can be calculated based on a size-dependent equation also modeled by W. W. Yu *et. al*.. This equation uses the diameter previously calculated and can be seen here:

$$\varepsilon = 5857\ (D)^{2.65}$$

The extinction coefficient can then be used to calculate the concentration of each sample solution using the Beer-Lambert Law (A=εbc). That is, the absorption value (A) at the same λ used in Equation 1.1 is equal to the extinction coefficient (ε) multiplied by the path length of the cuvette (b) and the concentration of the sample (c). It is important to note that the FWHM of the peak can invalidate diameter calculations if it is profoundly wider than 25 nm. It is notable that different ligands (e.g. Tiroctylphosphine oxide,

pyridine, and many thiols) bound to the QD surface are reported to have little to no effect on the calculation of the extinction coefficient [8]. The QD concentration and diameter was used to determine the amount of Zn and S needed to coat effectively in the next synthesis step (*i.e.* ZnS Coating).

One concern of CdSe core integrity is the potential of degradation upon exposure to atmospheric oxygen. While short periods (<10 min) of exposure to air did not result in noticeable decreases in QD quality, longer times can result in oxidation and degradation of the CdSe QD cores into CdO and SeO_2 (Figure 1.2). To prevent this degradation, ZnS is added as a shell coating.

The ZnS shell is added as quickly as possible after core synthesis to avoid oxidation [10]. A ZnS layer of at least 1.3 monolayers (MLs) has been shown in previous work to be the minimal coating to prevent degradation. Up to four additional ZnS MLs were added to increase the quantum yield and fluorescence intensity [11]. More than four MLs has been shown to decrease the fluorescence and quantum yield [12].

The addition of a shell is a commonly used method to increase fluorescence intensity and protect cores from degradation over time. In many cases, increases in quantum yield have been shown to be as much as ten times the yield of non-shell coated cores 5. When choosing the identity of the shell, a small lattice mismatch between cores (CdSe) and shells (ZnS) is the key to an effective shell coating. This mismatch allows the shell system to evenly coat the core without disrupting the lattice of the core system. The band gap difference of the shell can be adjusted to control where electrons are most likely to recombine in the core-shell system. Relaxation of electrons can be isolated within the core, within the shell, or within the core-shell interface, depending on the type of shell

system used.

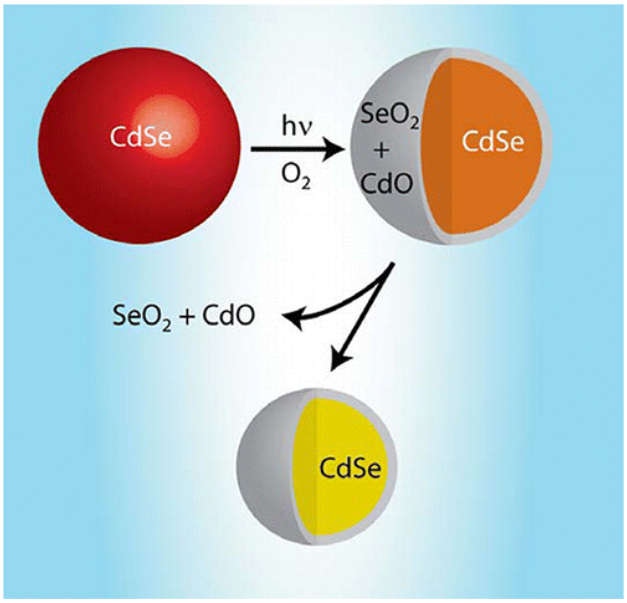

Figure 1.2. Oxidation of CdSe Cores. [13] Prolonged exposure of CdSe nanocrystals to oxygen in the atmosphere can lead to degradation. This degradation is observable as a blue shift in fluorescence emission (*i.e.* from bright red to yellow or orange fluorescence). Prolonged exposure can lead to complete quenching of fluorescence.

The band gaps of cores and shells can be selected to tailor the lowest energy recombination to the area of interest. Confinement of electrons to the core can be chosen by selecting a shell with an increased band gap compared to the core. Increasing the band gap of the shell causes electrons to recombine within the core. This is what is referred to as the Type I core-shell system. CdSe-ZnS QDs (the focus of this work) are examples of type I core-shell systems. Spatially confining electrons within the core decreases relaxation through non-radiative processes. Other core-shell types (Figure 1.3) include Type II, in which the valence and conduction band of the shell are either above or below their respective bands in the core. This results in an isolation of electrons within the core-shell interface. Reverse Type I core-shell systems have a smaller band gap in the shell

than the core. This causes an isolation of electrons within the shell instead of the core.

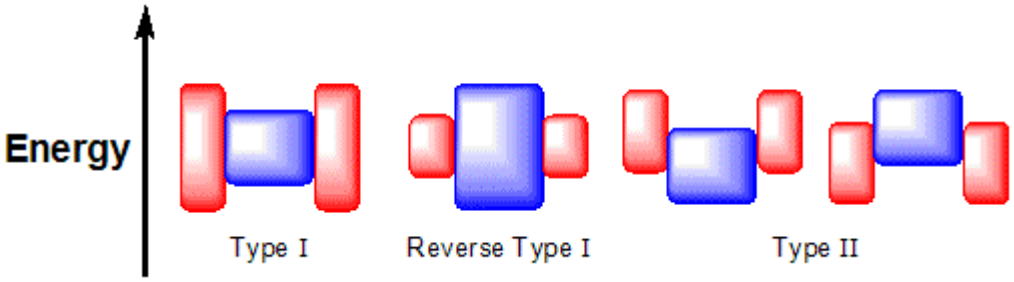

Figure 1.3. Core-Shell System Types[3]. Core-shell system types confine electrons to a specific region within the QD structure.This is done by adjusting the core band gap (Blue) and the shell band gap (Red). This can increase the quality of the QD by isolating the ability of an electron to recombine, which may decrease trap states.

Another layer of complexity to QD structure is the characteristic interaction of organic ligands with the surface. A multitude of ligands, such as trioctylphosphine oxide (TOPO), tetradecylphosphionc acid (TDPA), and dithiol compounds, are used to impart specific functionality or stability[14]. Ligands bind to the outside of the shell through dative bonds. This bond with the surface of the QD core is formed through oxygen, sulfur or another electronegative element of the ligand[10]. The ligands also contain hydrophobic moieties that interact with organic solvents, typical of QD synthesis conditions. These hydrophobic moieties limit the utility of QDs by restricting the QDs to non-polar solvents. Consequently, further modification is needed before QDs can be used in living systems.

Modifications to impart QDs with water solubility must be made before they can be applied in most living systems. To this end, there are three major techniques used: ligand exchange, surface silanization, and coating with amphiphilic polymers. Each of these techniques has advantages and shortcomings in regard to stabilization, overall size,

or ease of functionalization.

A popular technique to impart water solubility to QDs is ligand exchange. Ligand exchange works by thermodynamic competition between two ligands for surface binding. Trioctylphosphine oxide (TOPO) is a common ligand of QD cores since it is a byproduct of core synthesis. However, when more stable ligands compete for shell interaction, TOPO can be replaced [15]. Many thiols are commonly used for ligand exchange with TOPO. Compounds containing multiple thiol groups (such as dihydrolipoic acid, Figure 1.4) can datively bind to the shell multiple times from a single ligand (*i.e.* multivalent), increasing stability [16]. Ligand exchange may suffer from decreased stability in water compared to other water solubilization methods. This is the result of the hydrolysis of ligands over time, leading to dissociation from the QD surface. Current work in other projects in our lab are attempting to increase the stability of ligand-QD associations by using multiple dative bonds through a single ligand [16].

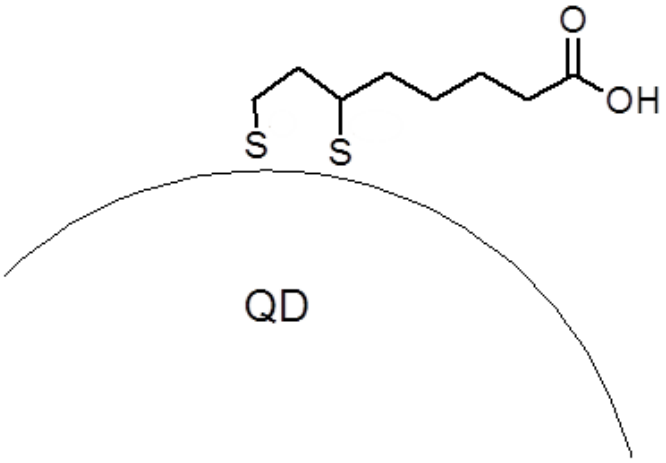

Figure 1.4. Surface Interaction of Bidentate Thiol Ligands. Ligand exchange methods attempt to increase the surface interactions of many ligands by creating multiple dative bonds to the surface.

A second method to impart water solubility is surface silanization. This method uses compounds containing trimethoxysilane groups that can be cross-linked to form siloxane bonds to create a shell that can be further functionalized [16]. This type of shell network is much more stable for long-term storage than ligand exchange. However, this extensive shell increases QD size more than stabilization via an amphiphilic polymer or ligand exchange methods [16]. Silanization also requires much more intensive procedural considerations than ligand exchange or amphiphilic polymer interactions.

Amphiphilic polymer interactions are the newest of the three common techniques used to impart water solubility to QDs. This method relies on hydrophobic/hydrophilic interactions between the polymer and the ligand coating the surface of the CdSe/ZnS core-shell. The three branching long carbon chains of the TOPO ligand interact with the hydrophobic portion of the amphiphilic polymer. The result is a micelle-like structure (Figure 1.5) that imparts water solubility to the QD with hydrophilic functional groups on the outside of the polymer. This method is much less labor intensive than the silanization, while maintaining resistance to enzymatic degradation and hydrolysis [17]. The amphiphilic polymer can be chosen to contain chemical moieties for future bioconjugation. Amphiphilic polymer interaction was chosen as the water solubility method in this work for its longer stability times vs. ligand exchange and small size vs. surface silanization.

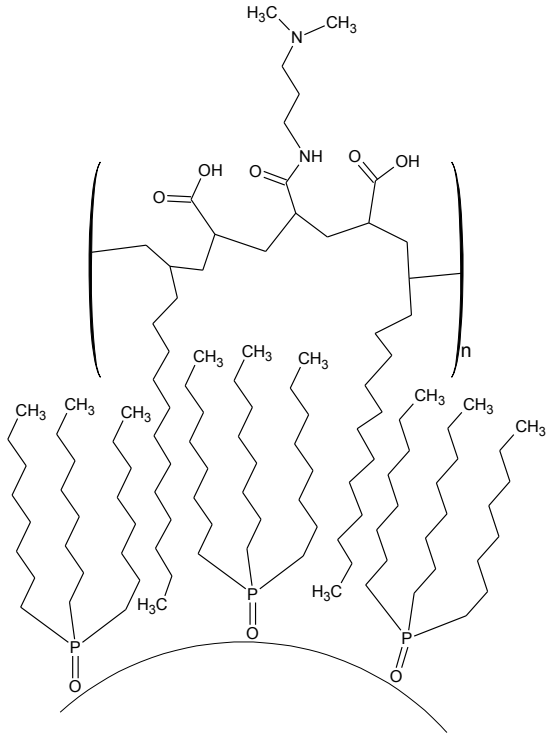

Figure 1.5. Interaction of an Amphiphilic Polymer with a QD Surface. The hydrophobic chains of the amphiphilic polymer integrate with the hydrophobic chains of the TOPO, which are datively bound to the QD surface. This exposes the hydrophilic moieties of the amphiphilic polymer as the new "coating", imparting water solubility to the QD.

1.2 Gene Therapy

Gene therapy has been the focus in many genetic disease treatments (*e.g.* severe combined immunodeficiencies, SCIDs) within the past few decades [18]. The main goal of gene therapy is to treat diseases that are the result of a genetic disorder, mutated genes, or faulty/missing proteins. Gene therapy inserts the missing or functional version of the gene into the cell and replaces the mutated or missing one. Viral gene therapy in particular has been shown to be one of the most efficient methods [18]. However, non-viral techniques are being developed because of the safety concerns of viral techniques [18].

Viral gene therapy can be an extremely effective technique that has improved the

treatment of diseases, such as SCIDs, by modifying a virus to insert therapeutic DNA. This success has been achieved in some clinical trials by using a disabled retrovirus as a vector [18.] This disabled virus can utilize its natural ability to efficiently deliver a gene to the nucleus. The common viruses used in gene therapy are the adenovirus, retrovirus, or herpes simplex virus [19]. To ensure that viruses are safe for gene therapy they are genetically modified to remove or disrupt coding sequences that could cause dangerous side effects. In its first years, gene therapy looked very promising, but in 2002 patients receiving treatment in France developed leukemia-like symptoms [18]. This caused a new wave of research and concern that ended with the realization that the virus was able to easily insert the therapeutic sequences. However, insertion can promote or disrupted many regulatory genes within the cell. In the case of the leukemia patients, the gene disrupted a sequence that affected apoptosis, leading to uncontrolled cell replication (*i.e.* cancer) [18]. Another disadvantage of viral gene delivery is the storage capabilities of the vector. Many viral vectors have a very limited capacity for carrying therapeutic DNA, meaning the larger therapeutic sequences may not fit within the viral capsid [20.]

Alternative non-viral methods (*e.g.* transfection via lipoplexes and polyplexes) have been developed to avoid many viral complications. The main goal of lipoplex or polyplex formation is to compact and protect therapeutic DNA from degradation during cellular delivery and intracellular trafficking to target locations. Lipoplexes (complexes between cationic lipids and anionic phosphate backbone of nucleic acid sequences) are micelle-like structures that can be functionalized for cellular interactions [21]. Positively-charged formations bind DNA through electrostatic interactions due to the negative charge of polyanionic DNA. A common example of a cationic lipid vector is the

commercial transfection reagent lipofectamine, which electrostatically complexes DNA to form a lipoplex [22]. The lipoplex can fuse with the plasma membrane of cells to release DNA into the cytosol. While this is effective, transfection relies on the ability of DNA to enter the nucleus [21]. However, lipofection remains the most common non-viral gene transfer technique used in clinical trials [23].

In contrast to lipoplex formation, polyplexes utilize a cationic polymer for electrostatic binding and condensation of DNA. The resulting polyplex structure is amorphous. Polyplexes are generally able to condense DNA at a much higher efficiency that lipoplexes [21.] As long as the polyplex maintains a net positive charge, it retains that ability to interact with the membrane of the cell [21]. Polyplexes are often taken up by endocytosis to a larger degree than direct insertion through the plasma membrane.

All non-viral methods have strengths and weaknesses, but shared challenges arise from how these vectors are intracellularly trafficked to the nucleus of the cell [24]. Once internalized by the cell, vectors can go through many pathways that include clathrin-mediated endocytosis, caveolae-mediated endocytosis, or macropinocytosis [24]. Macropinocytosis is largely ignored in this work due to it internalizing primarily structures over 500 nm in size [24] .Clathrin and caveolin-mediated endocytosis are the primary trafficking pathways suspected for QD vectors. Clathrin-mediated endocytosis allows for specific contents to be internalized and is often triggered through specific receptor proteins on the plasma membrane of the cell. The protein that coats the outside of this type of vesicle is clathrin. Caveolin-mediated endocytosis is a less common mechanism of internalization that does not depend on clathrin, but instead caveolin. This pathway is known to be associated with the internalization of animal viruses [25]. These

two endocytic pathways can lead to the Golgi apparatus and eventually into the nucleus through a hypothetical pathway proposed by Dr. Fichter (Figure 1.6). However, this pathway relies on the ability to avoid lysosomal degradation. If the contents are delivered to lysosomes, they will be subjected to a highly acidic environment and degradative enzymes that can digest therapeutic DNA. Many conjugates can go through both pathways, which can lead to significant lysosomal degradation unless a targeting domain is added to avoid the lysosome [26]. With the addition of a targeting agent, non-viral vector contents could be targeted through early endosomes into the Golgi, from the Golgi to the endoplasmic reticulum, and from the endoplasmic reticulum into the nucleus.

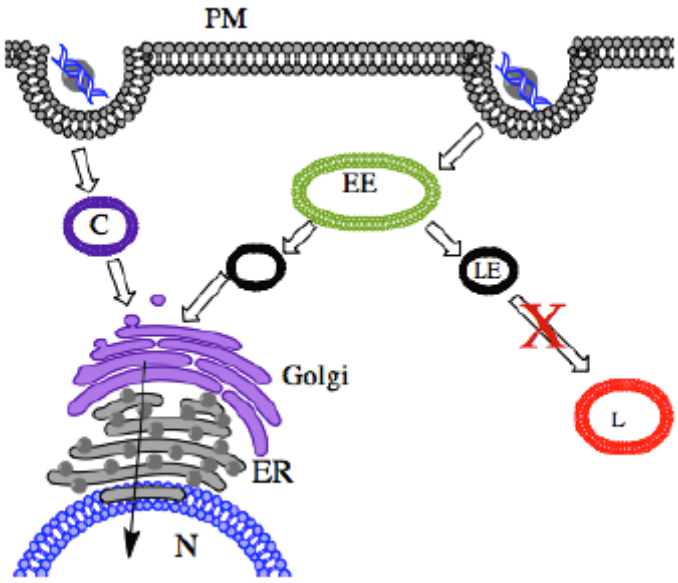

Figure 1.6. Potential Pathways of Non-Viral Gene Delivery. The goal of this work is to exploit a targeting molecule that can direct the therapeutic QD-DNA vector taken from the plasma membrane of the cell (PM) through the early endosome (EE) or caveolae (C), and into the Golgi apparatus. The Golgi can then traffick the contents through the endoplasmic reticulum (ER) and into the space between the inner and outer nuclear membrane, which is contiguous with the ER. The effectiveness of this technique hinges on the ability of the targeting molecule to avoid trafficking to lysosomes (L). Image obtained from Dr. Katye Fichter (manuscript in progress).

A main strategy to avoid lysosomes is conjugation of biomolecules to direct the vector once inside the cell, avoiding the lysosome entirely. To this end, many types of surface functionalization of QDs have been explored. This work focuses on attachment of a protein, wheat germ agglutinin (WGA), to the QD surface for direction within the cell; along with the attachment of polyethyleneglycol (PEG) derivatives to reduce non-specific binding [27, 28]. By attaching WGA and PEG we hope to avoid lysosomal degradation while directing the complex to the nucleus of the cell.

1.3 Biological Applications of Quantum Dots

Many fluorophores (organic dyes, fluorescently conjugated antibodies, or more recent fluorescent nanoparticles) are used to label structures within cells. Each of these probes have advantages and disadvantages considering imaging time, specificity, and application to living cells. These fluorescent markers can be used in conjunction with one another to create a more thorough view of the cell.

While traditional organic dyes, like Hoechst, and DyLight™ are relatively small in size, they have limited photostability, which limits the effective imaging time [29]. The fluorescence lifetime of most organic dyes are only around 5 ns, while QDs can attain 100+ ns [30]. This allows for more sensitive data to be obtained over longer imaging time periods [30]. QDs also resist photobleaching, which allows imaging over the course of hours when properly utilized. Fluorophores like Hoechst and DyLight™ may quench within seconds upon exposure to irradiation. After ~10 min, in some cases, the fluorescence of these fluorophores can be completely quenched, making them inefficient for long-term

imaging. The use of QDs is a suitable alternative to avoid the photobleaching of organic dyes.

Immunoglobulin G (IgG) antibodies have been used to selectively bind to proteins that are specific to organelles within cells. Their structure (seen in Figure 1.7) consists of Y shape formed by two heavy and two light chains of peptides. These chains form regions called the F_{ab} and F_c regions. The F_{ab} region is where the specific binding to an antigen takes place, while the F_c region is highly conserved among the same species. IgGs are harvested from sera of animals (mouse, rat, goat, horse, etc) treated with an antigen [31]. For example, a rabbit anti-giantin antibody is a Golgi apparatus marker. This particular antibody is harvested from a rabbit, and selectively binds giantin, a protein found in the Golgi's membrane. Primary antibodies such as this are specific to a protein of interest such as giantin, but not always fluorescently conjugated. To visualize the antibodies with a microscope, a secondary antibody is used that binds to the primary antibody. The secondary antibody is conjugated to a fluorescent molecule such as Dylight™ to allow visualization. While primary antibodies bind to antigenic epitopes present on a protein of interest, secondary antibodies bind to the primary antibodies. An example of this kind of antibody is DyLight™ 550-conjugated goat anti-rabbit IgG. This antibody was harvested from a goat, and binds specifically to rabbit IgG. Overall, the resulting sequence is a cell labeled with a rabbit IgG specific to giantin, which is subsequently recognized by a goat anti-rabbit antibody conjugated to DyLight™ 550 (Figure 1.8). The secondary antibody binds to the primary antibody, allowing for a fluorescent signal to be produced under the microscope when excited.

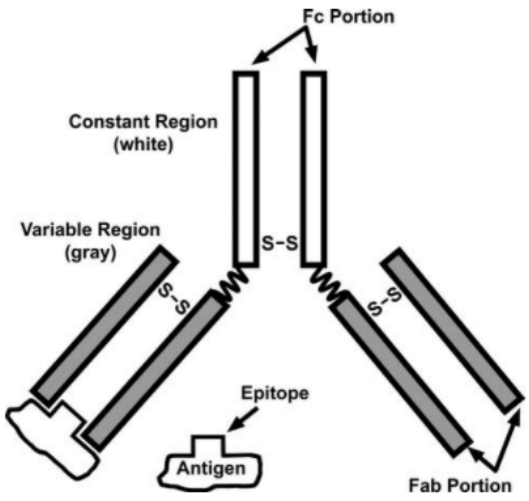

Figure 1.7. General Structure of an Immunoglobulin G (IgG) [32]. IgGs consist of two heavy chains and two light chains in a Y formation. The central portion of the Y shape is a highly conserved region call the F_c region (Top). The two arms of the Y (Bottom) contain the F_{ab} region, which is highly variable so as to only bind to specific epitopes.

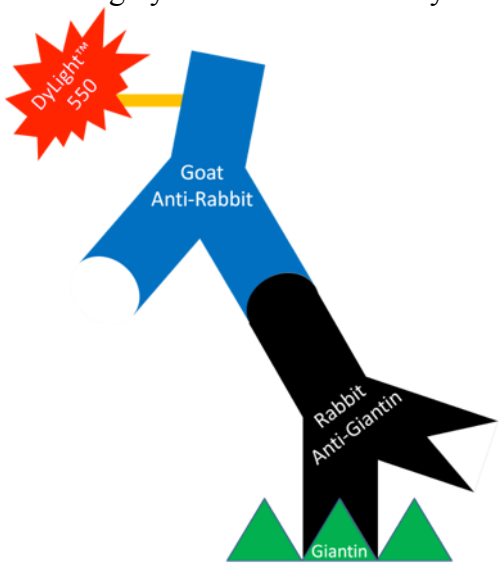

Figure 1.8. Sequential Antibody Binding Scheme used in Immunocytochemistry (ICC). Many primary antibodies (here, rabbit anti-giantin) do not have fluorescent tags to make them visible in fluorescence microscopy. To be able to visualize these antibodies, a secondary antibody (e.g. goat anti-rabbit) is used that specifically recognizes the primary antibody, and is chemically conjugated to a fluorescent tag (*e.g.* DyLight™ 550 needed for visualization).

1.4 Mammalian Cell Culture

A key component of cell studies is the ability to grow consistent and reproducible cell lines within the laboratory. This requires a careful monitoring of cellular environments and aseptic technique to prevent contamination. To this end, all solutions and materials used in living cell work must be sterilized and kept in a dedicated cell culture hood. Standard sterile technique protocols were practiced and cells were carefully monitored for growth rate, morphology and any potential contamination.

Over the course of experimentation, HeLa (Human cervical cancer) and N2a (mouse neuroblastoma) cells were grown and split once every 2-3 days to maintain a cellular environment suitable for exponential growth. It is important that cells do not become confluent in order to maintain desired functionalities. N2a cells were split approximately 1:5 every 2-3 days to maintain exponential growth conditions, while HeLa grew slightly faster, and were split every other day. The cells were split when they reached about 80% confluency. Above this density normal cellular function can be lost from outside pressures. That is, cells that survive thrive in harsh conditions, and no longer represent cellular traits of the cell line selected.

1.5 Microscopy

Understanding microscope capabilities and limitations is fundamental to drawing accurate conclusions from cellular trafficking studies. Imaging of cells was performed using an inverted fluorescence microscope from Zeiss with an adapter for a camera. This basic setup views the sample from below, allowing for visualization of samples in media that could damage the objective in an upright scope. An upright scope views samples

from above, making it better for samples such as conventional glass slides when media is unnecessary. Depending on sample types, either an upright or inverted scopes is preferred for more defined images.

Filter cubes must be fitted into the fluorescence microscope to select proper wavelengths necessary to view the fluorophore used in the experiment. Many fluorophores used as cellular labels have a very distinct excitation and emission wavelengths. To excite specific fluorophores, an excitation source with a broad spectrum of light between 280-800 nm is used [33]. This light is directed into the microscope to the filter cube and passed through an excitation filter so that only wavelengths that excite the fluorophore reach the sample. Similarly, light emitted from the sample can be selected for specific emission wavelengths. The combination allows for a specific fluorophore to be viewed by using each specific filter cube.

Each filter cube consists of three parts: an excitation filter, an emission filter and a dichromatic mirror [34](Figure 1.9). Excitation filters allow a specific, narrow range of wavelengths to pass through. The selected wavelengths of light then hit a dichroic mirror that reflects the desired wavelength range towards the sample; all other wavelengths of light do not pass through the filter and are therefore not directed to the sample. The light then excites the fluorophore in the sample, which causes fluorescence and emission of light that is typically red-shifted from the excitation light. While fluorescence is emitted in all directions, some of the light emitted passes down from the specimen through the dichroic mirror and through an emission filter. The emission filter only allows light in the wavelengths emitted from the fluorophore of interest to pass through and ultimately reach the oculars or the camera. All other wavelengths of light cannot pass through.

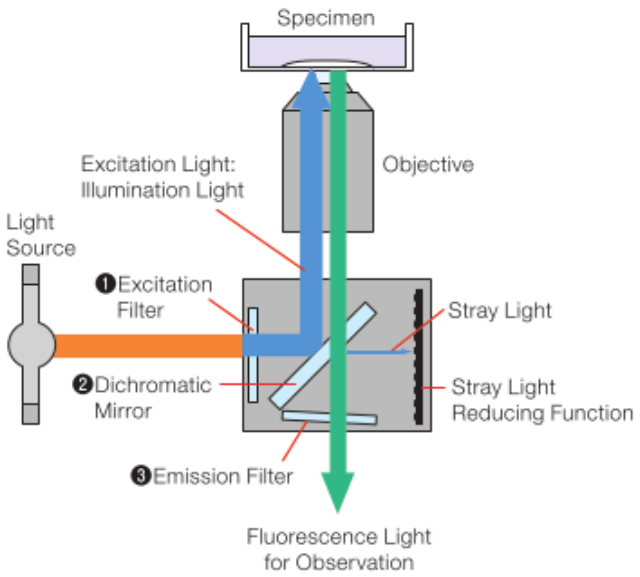

Figure 1.9. Light Path through a Filter Cube in an Inverted Fluorescence Microscope [34]. To obtain a clear image of light emitted from a specific fluorophore in a sample, it is essential to block other fluorophores form appearing in the image. To achieve this, a filter cube is used to screen the light source (Pictured above as orange) and allows a narrow range of wavelengths (Pictured as blue) to hit the specimen. Once excited, the fluorophore in the sample emits specific wavelengths of light (Pictured as green) that can pass through an emission filter. The emission filter also blocks any undesired wavelengths of light (room light, other fluorophores, etc) from reaching the detector.

Different filter cubes can be used to focus on specific fluorescence sources as long as there is little overlap between the excitation and emission wavelengths. Many fluorophores can only be excited by a small range of wavelengths, while emitting in a small range of wavelengths as well. Fluorophores that significantly overlap in either of these cases cannot be used in the same experiment or bleedover (*i.e.* signals from other fluorophores in the sample) can cause erroneous signals. QDs are a strong tool for fluorescence image analysis due to the ability to be excited by a wide range of wavelengths, with a very narrow band of emitted wavelengths. This makes QDs very attractive for co-localization studies where multiple fluorophores need to be visualized at

the same time.

Co-localization analysis is used to determine if the signal collected from two different fluorophores originated at the same location in the sample. There are many different techniques to calculate the degree of overlap between two signals [35]. The technique used must be carefully selected depending on the nature of the sample and the specific data desired. For this experiment, we evaluated the degree of overlap between the signals from two fluorophores using what is called the Manders' coefficient [4]. This calculation can be seen here:

$$M_i = \frac{\sum R_{i,coloc}}{\sum R_i}$$

R_i is the occurrence of a specific fluorescence signal, while $R_{i,coloc}$ is the occurrence of that signal overlapped with a second signal of interest. M_i is a value between 1 (indicating completely positive correlation) and 0 (indicating completely exclusive correlation) [35].

The Manders' coefficient allows for a quantitative measure of the degree of overlap between two fluorophores when the two images are overlaid using an image processing software (e.g. ImageJ). The Manders' coefficient was chosen for co-localization analysis in this work for the ability to emphasize the importance of one signal over another. In this case, QDs are the signal of focus. That is, the degree the QD signal overlaps with the organelle marker signal (e.g. Golgi apparatus, lysosomes) is of greater interest than the degree the organelle signal overlaps with the QD signal. In short, this analysis does not include the potentially large signal from organelles that do not overlap with the QD signal (*e.g.* some lysosomes that do not contain QDs). It only returns information about the QD signal and its degree of overlap from the organelle marker

signal.

This work hopes to achieve a high quality synthesis of QDs for further modification. The QDs are then functionalized to act as nanocarriers for DNA delivery to a targeted area of the cell (Nucleus). In this way the QDs could act as a therapeutic DNA delivery vehicle for targeted gene therapy methods.

CHAPTER 2: EXPERIMENTAL

2.1 Chemical List

All materials were purchased from Sigma-Aldrich (St. Louis, MO) unless otherwise specified. Acetone (wash grade), cadmium oxide (Cat. No. 202894), agarose (MidSci, Cat. No. BE-A125), 3-dimethlamino-1-propylamine (DMAPA) (Cat. No. D158003), 4-(4,6-dimethoxy-1,3,5-triazin-2-yl)-4-methylmorpholinium chloride (DMTMM) (Cat. No. 749613), hexanes (EMD Millipore, Cat No. 110-54-3), N-(2-Aminoethyl)maleimide trifluoroacetate salt (Cat No. 56951), 3-(N-morpholino)propanesulfonic acid (MOPS) (Fisher Bioreagents Cat. No. BP308-500), octadecene (Acros, Cat. No. 112-88-9), oleic acid (Cat. No. 364525), oleylamine (Acros, Cat. No. 112-90-3), paraformaldehyde (PFA) (Cat. No. 158127), phosphate buffer saline (PBS) (Thermo Scientific, Cat. No. SH30028.02), polyethylene glycol (PEG) derivatives (Creative PEGworks, $_2$HN-(PEG)$_{2000}$-CH$_3$ ["mPEG"] Cat. No. PLS-269, $_2$HN-(PEG)$_{2000}$-COO$^-$ ["cPEG"] Cat. No. PHB-930 (cPEG)), commercially available under the name poly(maleic anhydride-alt-1-tetradecene), 3-(dimethylamino)-1-propylamine derivative (from here on referred to as PMAL-d) (Cat. No. 90771), selenium powder (Cat. No. 229865), sulfur powder (Cat. No. 84683), tetrahydrofuran (THF) (Cat. No. 401757), trioctylphosphine oxide (TOPO) (Strem Chemicals, Cat. No. 78-50-2), Triton X-100 (Astoria-Pacific, Cat. No. 90-0770-04), wheat germ agglutinin (WGA) (Cat. No. 61767), zinc oxide (Cat. No. 96479).

For mammalian cell culture work the following biological reagents were purchased: pGFP-EEA1 (plasmid DNA encoding enhanced green fluorescent protein

fused to EEA1, AddGene Cat. No. 42307), Dulbecco's-Modified Eagle's medium (D-MEM) (Thermo Scientific, Cat. No. SH30022.01), Opti-MEM reduced serum medium (Life Technologies, Cat. No. 51985-034), rabbit anti-giantin antibody (Golgi Apparatus Marker, Abcam, Cat. no. ab24586), Dylight™ goat anti-rabbit IgG 550 conjugate (Thermo Scientific, Cat. No. 84541), LysoTracker (Molecular Probes, Cat. No. L7526), fetal bovine serum (Hyclone, Cat. No. SH30396.02) antibiodic/antimicotic solution 100X (Penicillin G, Streptomycin, and Amphotericin B) (Hyclone, Cat. No. SV30079.01), trypsin (Hyclone, Cat. No.AV30031.01), trypan blue (Hyclone, Cat. No. AV30084.01) and SYBR® Green (Life Technologies, Cat. No. S-7563). N2a (mouse neuroblastoma) cells and HeLa (human cervical cancer) cells were a kind gift from Dr. Tania Q. Vu at Oregon Health and Science University and Dr Paul Durham at Missouri State University respectively.

2.2 QD CdSe Core Synthesis

The Se precursor for CdSe QD cores was synthesized by adding 33 mg selenium powder to 5 mL octadecene in a sealed 50 mL round bottom flask. This mix was purged with a vacuum for 30 minutes and filled with nitrogen gas to avoid oxidation of trioctylphosphine in future synthesis steps. The mix was purged for ~20 min and then heated to 150 °C. The temperature was controlled with a thermocouple and proportional-integral-derivative (PID) controller to keep the temperature within +/- 2°C of the target temperature. The thermocouple and controller were calibrated with oleylamine/octadecene from 0 to 320 °C and found to be stable for at least 1 hour. After stabilizing the temperature for at least 10 min, 0.4 ml of trioctylphosphine was carefully

injected to prevent exposure to air. The black selenium powder fully dissolved as it reacted to form selenium trioctylphosphine, the Se precursor to the CdSe QD formation. The temperature was maintained at 150 ˚C until no visible selenium was left in the solution (Approximately 15 minutes).

The Cd precursor was synthesized by adding 19.5 mg of cadmium oxide to a 100 mL, 3 neck, RBF along with 25 mL of octadecene and 25 mL oleylamine. A mixture of octadecene and oleylamine was used as the solvent. This mixture was chosen because it was found to stabilize CdSe core formation and produce more consistent core quality than octadecene alone. Once the mixture was sealed, it was purged with argon gas. This setup allows for a condenser to be added, which minimized solvent loss due to evaporation while maintaining an inert atmosphere. The middle neck of the RBF was used to vent, while the other two necks were used for reagent injection and introduction of a thermocouple (see Figure 2.1). The heat was raised and stabilized to 150 °C and 0.9 ml of Oleic acid was injected to dissolve the cadmium oxide. The reddish powder fully dissolved to create a clear liquid, indicating the solution was ready for injection of the Se precursor to induce nanoparticle nucleation.

Once the Cd precursor solution was prepared in the reaction chamber, the solution was heated to 300 °C and stabilized for the duration of the reaction. Many trials were performed at temperatures as low as 250 °C and as high as 320 °C, but these temperatures yielded poorer quality cores. After the Cd precursor solution was stabilized at 300 °C, 1.5 ml of selenium-trioctylphosphine precursor was injected. The temperature initially dropped after injection, but the PID temperature controller stabilized the solution back to 300 °C within roughly 15-30 seconds. Samples of the product can be collected at regular

time intervals to ensure steady core growth. Using these reaction conditions, CdSe QD products were obtained with a fluorescence emission λ_{max} of 650 nm and, a very narrow full-width at half max (FWHM) of 25-30 nm, similar to that of commercially available QDs. CdSe cores were purified via precipitation with excess acetone (75 mL acetone for 25 mL QDs). This solution was then centrifuged at 12,000 x g for 1 hour. The precipitate was dissolved in hexane for longer storage and preparation for ZnS coatings. This wash process was repeated three times to ensure purification.

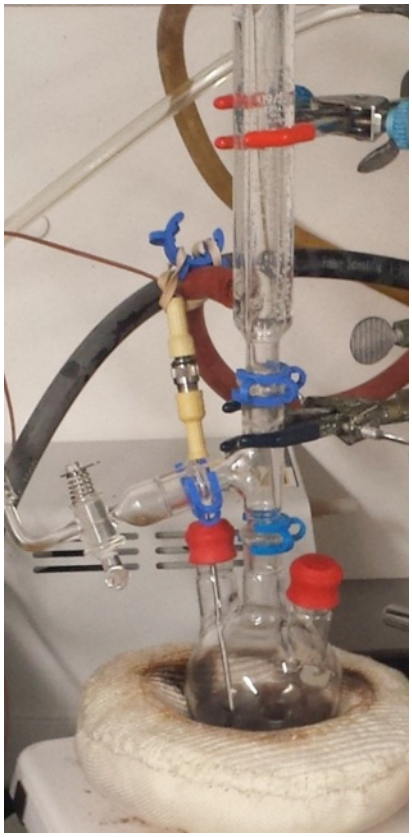

Figure 2.1. Reaction Setup for CdSe QD Synthesis. A three-neck RBF was used for ease of reagent injection, while simultaneously being able to monitor the reaction with a PID temperature controller and maintain an inert atmosphere. A second valve at the top of the condenser allowed for the reaction to be sealed or subjected to vacuum, as needed. This setup could also be adjusted from a 100 mL RBF up to 500 mL. However, it was found that an increase in reaction volume increased the size dispersity of the QD products.

2.3 Passivation of CdSe QDs with a ZnS Shell

A few different methods were attempted before settling on the most consistent ZnS shell coating procedure. The first attempts used a pyrophoric method and included the use of diethyl zinc and trimethylsiylsulfide (TMS) under an inert atmosphere. Without a glove box, this procedure may become very hazardous since the diethyl zinc reacts explosively with water and can easily catch fire upon contact with air. Additionally, TMS is a potent toxin with a very unpleasant smell. Mixed results were obtained with this reaction. Some trials achieved the growth desired, while other trials showed little-to-no growth (*i.e.* did not demonstrate the expected photoprotective effects of passivation when viewed on a fluorescence microscope). While this procedure has been previously published [36], and has worked for others, without the use of a gloves box, it became impractical to continue this technique for our purposes.

The most consistent method, and the one used most often in these experiments, was the Successive Ionic Layer Adsorption and Reaction (SILAR) method, suggested by Dr. Collin Heyes at the University of Arkansas. This method allows for a controlled addition of each layer of zinc and sulfur to the core. The Zn or S precursor solutions were prepared to coat 200 μL of CdSe QDs with a concentration of about 4 μM. The Zn precursor was a stock solution of zinc oxide (3.2 mg) dissolved in 18.2 mL octadecene and 1.8 mL oleic acid; the sulfur precursor solution was 102 mg elemental sulfur dissolved in 20 mL octadecene. Both precursor solutions were heated to 200 °C to dissolve fully. The zinc precursor was cooled to 80 °C while the sulfur precursor was allowed to return to room temperature. The injection volumes necessary for each

precursor injection were calculated using the lattice constant for ZnS and the diameter of CdSe cores.

The extinction coefficient and diameter of CdSe cores was determined using the first excitonic peak, as described in the introduction. The extinction coefficient and diameter are needed to calculate the concentrations of the CdSe solution. Once the current nanocrystals diameter is known, the expected diameter, with the addition of one monolayer (ML) of ZnS, can be calculated using the lattice constant for Wurtzite (*e.g.* ZnS, 0.626 nm). The difference in volume between a CdSe core and a core with single ML of ZnS, was calculated using the equation $V_{ML}=3/4\pi(R_{Total}-R_{core})^3$. The moles of precursor needed for each ML was calculated using the bulk density for ZnS (42,100 mol/m^3). Each injection was calculated this way, increasing the diameter of the core as needed to account for the additional MLs.

CdSe QD cores were brought to 150 °C and stabilized, and the calculated volume of zinc or sulfur precursor was injected to allow one full coating of the nanoparticle. The reaction was allowed to proceed for 15 min before the next injection. A total of 4 zinc layers and 4 sulfur layers were added in succession. After the last injection the temperature was allowed to cool to room temperature. The CdSe/ZnS nanocrystals were then washed using the same method for CdSe cores and centrifuged at 12,000 x g for 1 hour to remove any unreacted precursors. These cores were stored in hexanes to prepare for water solubility.

The SILAR method requires more time than the pyrophoric method mentioned above, but reduces the chance of ZnS nucleation and offers more synthetic control than bulk shell synthesis. A 5-10 nm growth is indicative of successful shell passivation. Type

1 core/shell systems have a characteristic 10 nm shift in fluorescence λ_{max} upon successful addition, which has been attributed to the "leaking" of electrons into the shell bands [1]. A shift in fluorescence λ_{max}, as well as resistance to photobleaching, are good indications of successful core passivation. These CdSe/ZnS QDs were visualized using a fluorescence microscope for up to 60 min with little-to-no noticeable photobleaching.

2.4 Imparting Water Solubility to CdSe/ZnS QDs

For QDs to be biologically relevant for gene therapy applications, they must be solubilized in water. There are many ways to accomplish this (previously described in Chapter 1). The use of an amphiphilic polymer was the primary focus of this work. Attempts were made to synthesize an amphiphilic polymer in-house with mixed results. It was quicker and cheaper to purchase an ideal polymer that was shown to be suitable in previous work [37]. Polymer synthesis was quick, but characterization and optimization of the degree of functionalization took longer than anticipated. The commercial polymer selected for water solubilization was purchased under the name Poly(maleic anhydride-alt-1-tetradecene), 3-(dimethylamino)-1-propylamine derivative (from here on reffered to as PMAL-d, Figure 2.2).

First attempts at water solubilization started with a mixture of CdSe/ZnS QDs (capped with TOPO), in octadecene, with a large excess of PMAL-d dissolved in water. The mixture was sonicated for one hour, with occasional vortexing. This method resulted in a portion of QDs stable in water, but a much larger portion was present as an insoluble QD precipitate. This precipitate made concentration calculations impossible for these

trials. A more efficient water solubilization method was needed to be able to account for the final concentrations of the QDs in water.

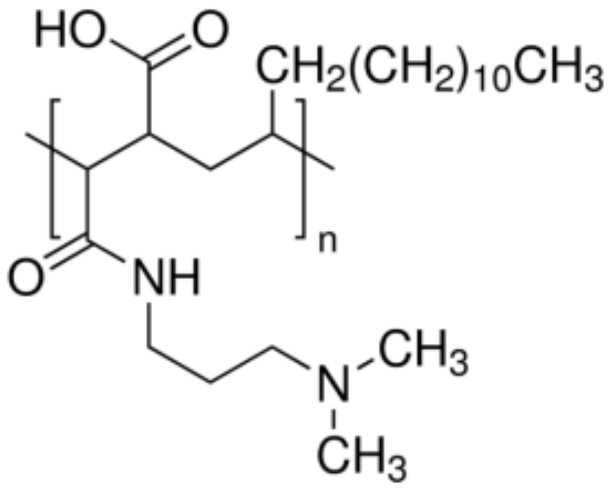

Figure 2.2. Chemical Structure of PMAL-d [38]. PMAL-d was used for the water solubilization of CdSe/ZnS QDs. Its long 12-carbon chain allows interaction with TOPO ligands bound to the QD surface. This polymer also has tertiary amine functionalization, which is protonatable at physiological pH, to impart some positive charge to the QD surface. Finally, carboxyl groups of this polymer can be used as "chemical handles" for further bioconjugation.

A paper published in Nature Protocols [17] offered an alternative method, which called for suspending the QDs in THF before adding PMAL-d. Excess THF was slowly evaporated off, using a rotary evaporator, during the mixing procedure, allowing for QDs to be suspended within the water more efficiently. In theory, the slower evaporation (typically 3-4 hours) allowed more time for the QDs to be wrapped in the polymer and increased overall yield of water-soluble QDs. As the organic layer evaporated, it became less and less energetically favorable for the QDs to stay within the shrinking organic layer. While this method showed promise, it was not without limitations: CdSe/ZnS QDs quenched if exposed to THF for too long. The exact length of time before quenching

varied between trials. We speculate this variability may be due to the individual quality of the QD products used (i.e. the existence of trap states on the surface of the QDs, or defects in ZnS coating). As the QD quality increased, the time before quenching was extended.

Before solubilization, QDs were precipitated from hexanes and washed. This was achieved by adding 30 mL acetone to the QDs (1mL of 4μM) and centrifuging at 12,000 x g for 15 minutes. If red fluorescence (from unprecipitated QDs) was detected in the acetone, the addition of acetone and spin would be repeated. The precipitated QDs were then dissolved in 20 mL THF. To ensure the QDs were fully dissolved, the solution was sonicated for ~15 min. Once the QDs were fully dissolved, 30 mL of ~1mg/mL PMAL-d in DI water was added to the QDs in a 100 mL RBF, and the solution was rotovaped with a dry ice/acetone trap. Once the majority of the THF evaporated (roughly 80%) the solution appeared turbid in nature; at this point 50 mL of DI water was added. The rest of the THF and most of the DI water was evaporated slowly over the course of ~3 hours, or until the solution reached the desired concentration. The water-soluble QDs were kept at a concentration of at least 500 nM to avoid long term storage issues.

In many cases, dialysis was needed to remove excess polymer from the water-soluble QDs, indicated by solution turbidity. The turbidity may have been due to the formation of micelles by excess polymer. To purify the solution, it was dialyzed using a membrane with a MWCO of 20,000 kDa against 0.1M borate buffer, pH 8.5. Successful purification was indicated by the lack of turbidity post-dialysis. The solution was then concentrated using a vacufuge.

The coating with amphiphilic polymer to impart water solubility was performed in these experiments for the simple nature of the reaction compared to strategies incorporating ligand exchange. The experimental setup was cheaper, and more importantly, easier to repeat due to the less intense experimental design.

2.5 Surface Modification of Water-Soluble CdSe/ZnS QDs

Once the QDs were stable in water, they must be able to interact with DNA. The plasmid pGFP-EEA1 was purchased from Addgene and encodes for a green fluorescent protein (GFP) early endosomal marker within mammalian cells. This marker is an N-terminal fusion protein of GFP to EEA1. The GFP fusion allows for the gene to act as a reporter gene to indicate successful gene transfer. This plasmid was used because circular pDNA is more resistant to enzymatic degradation than linear DNA. The bacterium *Escherichia coli* (*E. coli*), containing pGFP-EEA1was grown on lysogeny broth (LB) agar plates, containing 50 μg/mL kanamycin for plasmid maintenance, at 37°C overnight. This LB medium was composed of:

Tryptone – 10g

Yeast Extract – 5g

NaCl – 10g

H_2O (Distilled) – to bring final volume to 1000 mL

A single well isolated colony was transferred to a 5 mL liquid LB and grown at 37°C and 200 rpm for approximately 24 hours. After outgrowth, the pGFP-EEA1 plasmid was purified using the Gene Jet miniprep kit according to the manufacturers protocol (Thermo Scientific). The concentrations and purification of each collected

plasmid sample was calculated measuring the absorption at 260 nm and 280 nm by spectrophotometry. The recovered plasmid was stored at -20˚C in TBE buffer until needed. The first sample of replicated and purified plasmid was digested with *XbaI* and a combination of *Xhol/EcoRI* and separated by electrophoresis with a 0.4% agarose gel to verify plasmid identity.

The first QD conjugation consisted of two simultaneous reactions. In the first reaction, PMAL-d on the surface of the QDs was functionalized with tertiary amines to increase the surface charge. By imparting a positive charge on the QD surface, the QDs can electrostatically interact with polyanionic pDNA. While the amphiphilic polymer, PMAL-d, has some positive character (due to tertiary amines that are protonatable at physiological pH), an increase in the overall surface charge was found to be necessary to allow more pDNA to bind to the QD surface. To this end, PMAL-d on the surface of the QD, was functionalized with more tertiary amines in the form of 3-(dimethylamino)-1-propylamine (DMAPA).To accomplish this, carboxylate groups on the QD surface were activated with 4-(4,6-dimethoxy-1,3,5-triazin-2-yl)-4-methylmorpholinium chloride (DMTMM) using a stoichiometry of 10,000 DMTMM to 1 QD (See Figure 2.3) in 0.1M borate buffer. DMTMM acts as an intermediate to react the carboxylic acid functionalities on the polymer coating the QD with the secondary amine groups on the end of cPEG and mPEG.After reaction for 15 minutes, excess DMTMM and byproducts were removed from the solution by dialysis with a 20,000 MWCO membrane. After collecting the solution from dialysis, DMAPA was added and allowed to react. Simultaneously during the above reaction, two polyethylene glycol (PEG) derivatives, “mPEG” and “cPEG” (see chemical list for structure) were added, both a 2,000 x molar

excess to QDs. PEG derivatives decrease the nonspecific binding of the QD and functionalize the QDs with both methyl and carboxylate terminal groups. The stoichiometric ratio of DMTMM:QD was varied in each trial (ranging from 10,000 to 500,000) to optimize the amount of tertiary amine reacted to increase the positive surface charge of the QD enough to bind pDNA. Unreacted DMAPA and PEGs were removed by dialysis overnight.

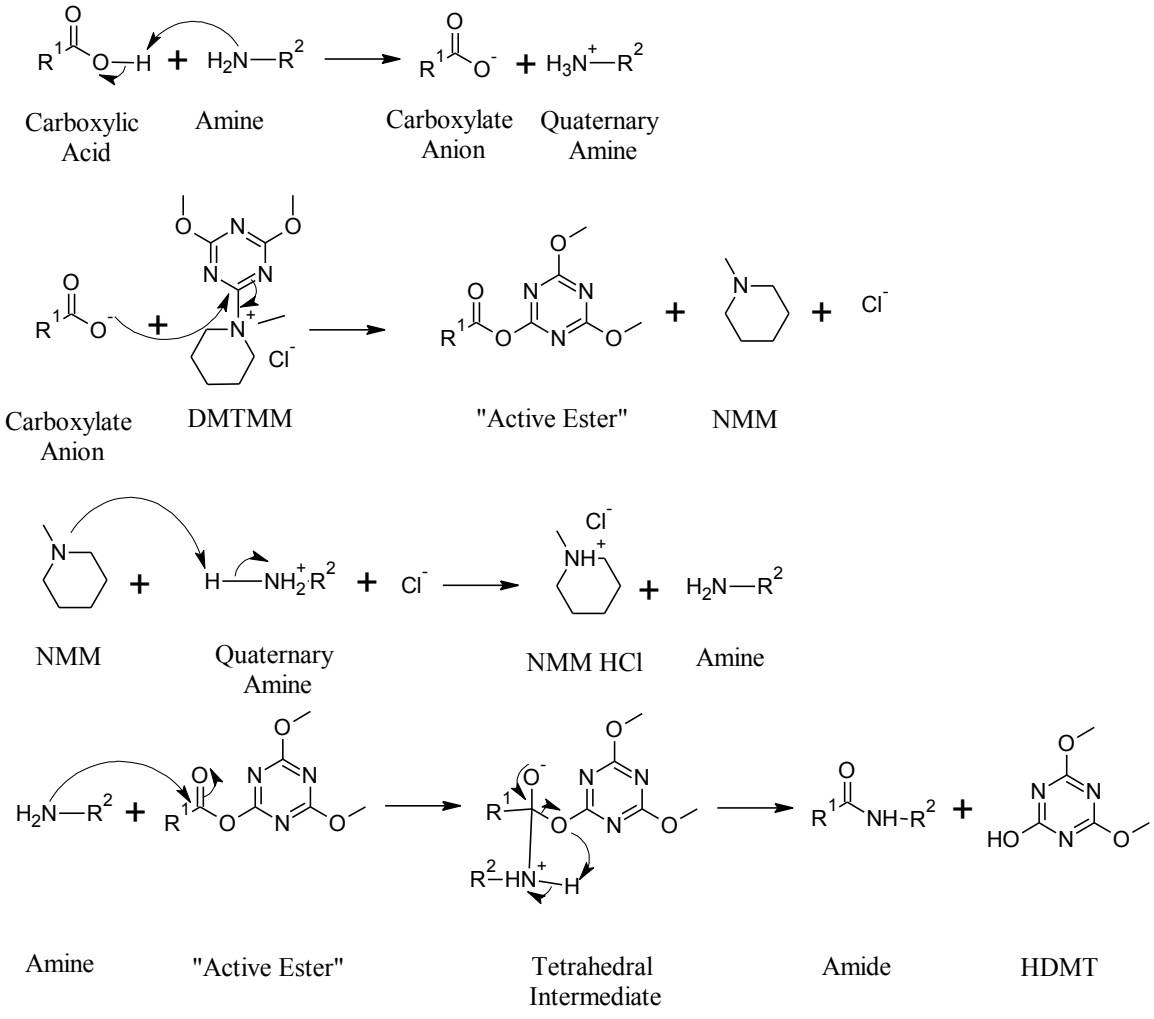

Figure 2.3. Mechanism of Activation of Carboxyl Groups by DMTMM [12]. DMTMM was used to activate the carboxylate groups of PMAL-d on the QD surface. Through this activation, other functionalization could be imparted to the surface through the reaction with a secondary amine.

Electrophoretic gels were used to evaluate ability of the QD-PEG/*tert*-amine conjugate to electrostatically bind negatively charged pDNA. The QD-PEG conjugates were evaluated on 0.4% agarose gels with SYBR® Green (a fluorescent DNA dye). The QD-PEG/*tert*-amine conjugates were incubated with ~0.1 μg pDNA at room temperature, for 30 min before loaded into the gel. The amount of QDs added to each trial was adjusted to evaluate electrostatic interaction of the DNA with QD-PEG/*tert*-amine Conjugates. The samples were electrophoresed 1 hour at 60 volts.

The surface charge of QD-PEG/*tert*-amine was evaluated using Zeta-potential measurements on a DLS instrument (Brookhaven Nicomp Model 380). A small sample of QD-PEG/*tert*-amine was diluted to 15 nM (in DI water) to evaluate the surface charge. The smallest portion possible was used since the technique is destructive to the QD-PEG/*tert*-amine sample.

2.6 Bioconjugation of QDs with Wheat Germ Agglutinin

Functionalized QDs may be able to bind pDNA, but need a trafficking group to guide the contents once within the cell. In an effort to target the pDNA payload to the cellular nucleus, QDs were bioconjugated to wheat germ agglutinin (WGA). WGA is a naturally occurring lectin that has been shown to bind to the nuclear envelope of the cell [39]. By attaching WGA to the QD-PEG/*tert*-amine conjugate, we hope to exploit natural endocytic pathways (Discussed in Chapter 1), to reach the nucleus of the cell. To achieve this goal, a two-step reaction scheme was developed to conjugate WGA to QD-PEG/*tert*-amine conjugate.

In the first reaction, the QD-PEG/*tert*-amine conjugate was reacted with maleimide to form a reactive intermediate that could bind to WGA. Terminal carboxylate groups from PMAL-d and cPEG on the QD surface were activated with DMTMM. A 10,000 x mole excess of DMTMM was reacted with QD conjugates for 5 min, then the solution was dialyzed over 10 min. After dialysis, N-(2-Aminoethyl)maleimide trifluoroacetate salt was added in a 100:1 mole excess (Figure 2.4, I and II). This conjugation creates a maleimide intermediate that can react with WGA. The maleimide derivative reacts with free sulfhydryl groups (*e.g.* in the form of cysteine side chains in a protein) at pH 7. Maleimides can also react with amines, but at pH 7.0 - 8.0 the reaction with free sulfhydryl groups is 1000x more favorable than with amines [40]. This reaction was performed in MOPS buffer at pH 7.4 to encourage reaction with sulfhydryl groups.

Once the maleimide reaction was completed, WGA (containing 4 free sulfhydryl groups [cysteine side chains] in its native, folded state) was added to the reaction (Figure 2.4, III, IV). A 2x molar excess of WGA was added in an attempt to prevent aggregation of multivalent products. The solution was allowed to react for 2 hours, and then a saturated cysteine solution was added to quench any remaining maleimide. The excess WGA and cysteine was removed using a 50,000 MWCO centrifugal filter.

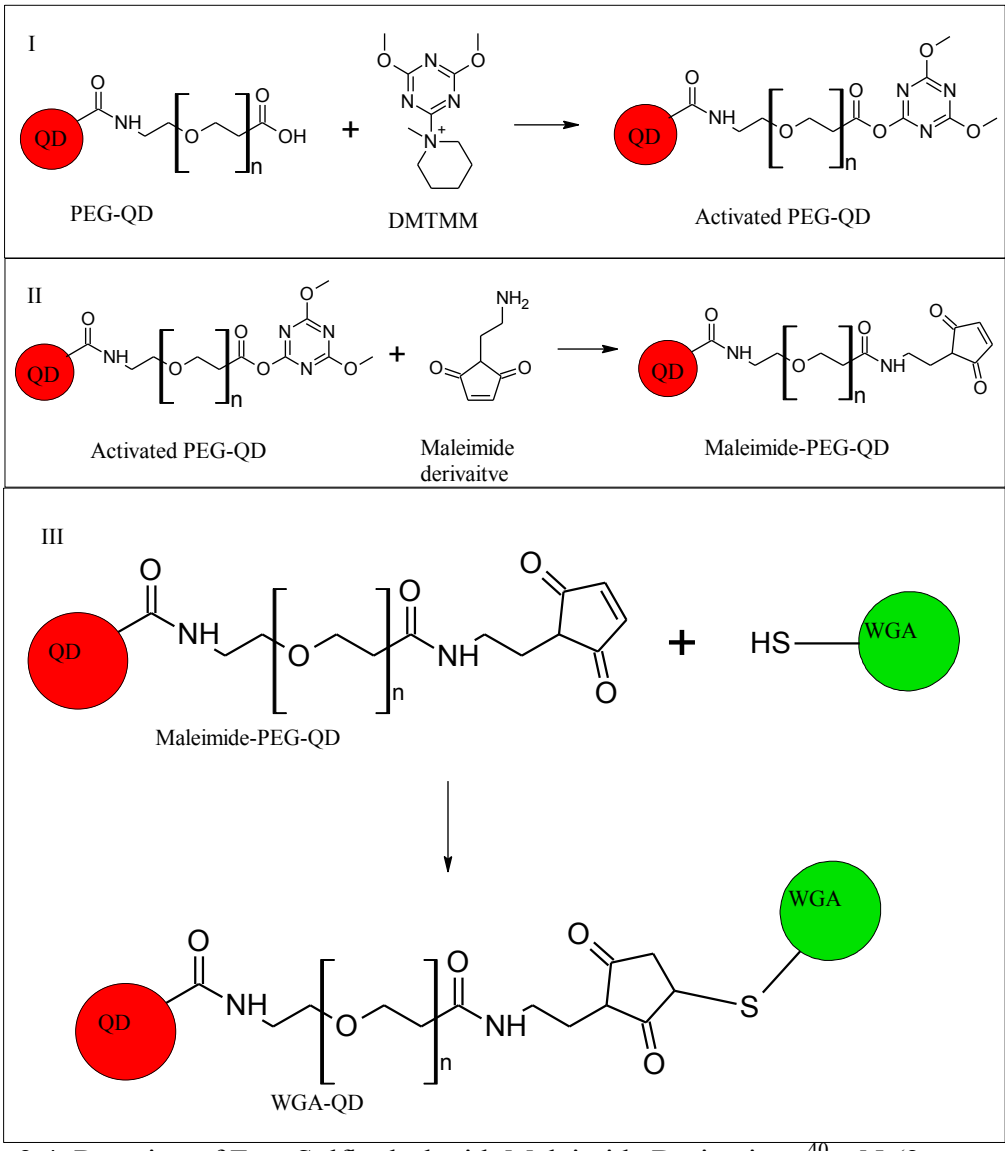

Figure 2.4. Reaction of Free Sulfhydryl with Maleimide Derivatives [40]. , N-(2-aminoethyl)maleimide was reacted with QD conjugates using DMTMM activation (I and II). The maleimide intermediate (product depicted in II) can undergo hydrolysis if left unreacted over longer periods of time. Therefore, Step III was carried out immediately after step II.

2.7 Cellular Interactions with WGA-QD Conjugates

Model cell lines were used to visualize the intracellular trafficking pathway of the WGA-QD conjugate. HeLa (Human Cervical Cancer) and N2a (Mouse Neuroblastoma, ATCC Cat #HB-12317) cells were split every 2-3 days at a 1:10 ratio. Cells were grown

in media consisting of 50% Dulbecco's Modified Eagle's Medium (DMEM) and 50% Opti-MEM supplemented with 10% fetal bovine serum (FBS) as well as 1X antibiotic and antimicotic solution (Penicillin G, Streptomycin, and Amphotericin B). N2a cells were plated in a 6 well plate containing a 25 mm^2 glass cover slip at a density of 50,000 cells per well and incubated for 1 day at 37 ˚C in a 5 % CO_2 atmosphere. Experiments to visualize live cell internalization of QDs, as well as visualization of cells fixed after timed QD-WGA conjugate internalization, were performed.

Two methods of visualization were used for living and fixed samples of cells. Ten μL of 40 nM QD-WGA conjugates were added to each well of cells. For live cell images, lysotracker (to visualize lysosomes) was added 20 min before the addition of the QD-WGA conjugate. The QD-WGA conjugate solution was added after placing the 25 mm^2 coverslip in a magnetic imaging chamber with cellular media so that the full internalization process could be observed in living N2a cells. Cells that were fixed were incubated with QD-WGA conjugates for 1 hour, 2 hours or 4 before fixation with 4% paraformaldehyde for 15 minutes. The fixed cells were stored in borate buffer (pH ~8.5) at 4°C. The following day the cells were permeabilized with 0.5% Trition X-100. Cells were blocked with 10% BSA for 1 hour, then treated with rabbit anti-giantin (Golgi marker) for 1 hour at a dilution of 1-1000 in 10% BSA (in PBS). After 1 hour the cells were washed 3 times with PBS buffer for 15 minutes. Afterward the cells were blocked again with 10% BSA for 1 hour before being treated with a secondary antibody DyLight 550™ goat anti-rabbit for 1 hour. The washing steps were repeated and the cells were stored in borate buffer pH 8.5. The coverslips were fitted into a magnetic imaging chamber for visualization under the fluorescence microscope.

A Zeiss Axio Observer microscope with a CCD camera (Zeiss axiocam Mrm) was used to visualize the cells. The microscope was equipped with filter sets: Rhodamine (ex545/em605), FITC (ex470/em525), and DAPI/Hoeschst (ex375/em460) and QD (ex460/em500LP) (Figure 2.5). Filter cubes were selected to visualize each fluorophore individually from the QD in each trial. The QD filter could not be used for visualization of QDs in the lysotracker experiment due to the co-excitation of lysotracker, leading to a possible false signal since the emission filter allows >500 nm to pass. Special attention was necessary to ensure the fluorescence signal from QD-WGA conjugates did not overlap with fluorescence signal from Lysotracker®. QD-WGA conjugates exhibited fluorescence emission at ~630 nm with a FWHM of roughly 30 nm. Specific excitation and emission filters were used to ensure these two signals did not overlap (Figure 2.6). For QD visualization a filter cube was assembled with a Rhodamine excitation filter (540 nm +/- 20 nm) and a Rhodamine red emission filter (610 nm +/- 40 nm). This allowed exclusive excitation of QDs and not the Lysotracker®. The use of a standard FITC cube (ex470/em525) was used to excite lysotracker. The final images were edited using ImageJ before being subjected to colocalization analysis using the Manders' coefficient plug-in.

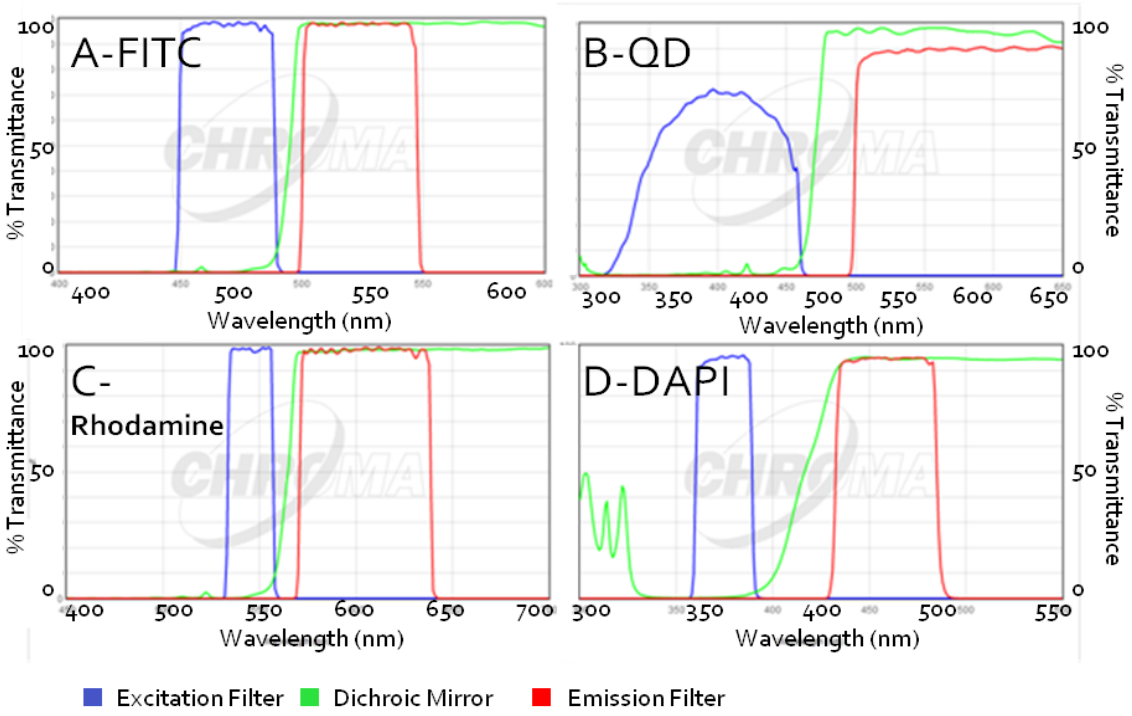

Figure 2.5. Filter Cube Excitation and Emission Cutoffs. Four different filter cubes were used for the fluorophores utilized in this work (Hoechst, QDs, Lysotracker, Dylight-550). FITC (A) was used to visualize lysotracker dye due to the lower emission filter (525 +/- 50 nm). QD filter (B) was used to visualize QDs for the long pass filter that allowed any emission over 500 to pass. Rhodamine (C) was used to visualize the QDs in the lysotracker trial to prevent excitation of lysotracker dye. Finally DAPI (D) was used to visualize Hoechst dye.

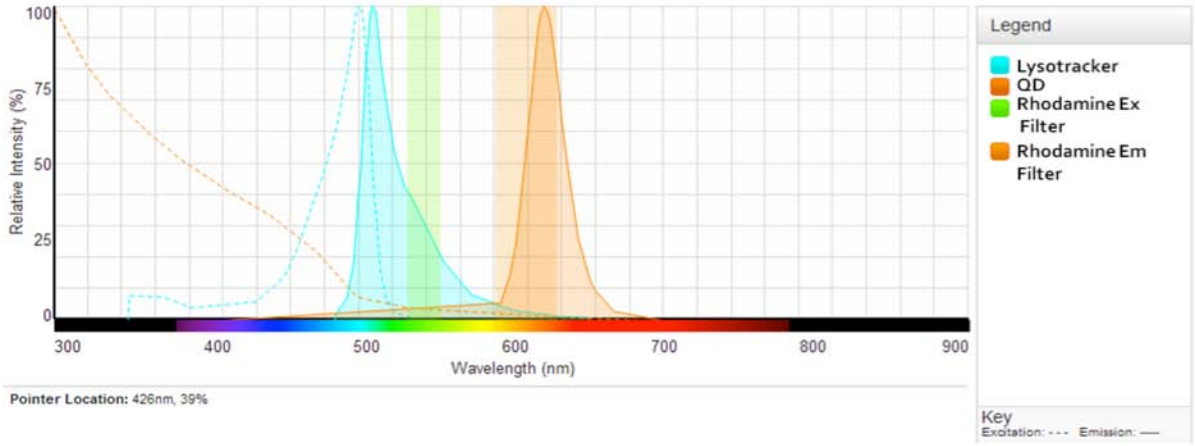

Figure 2.6. Excitation and Emission Spectra for Rhodamine Filter Cube Compared with Fluorescence Spectrum of Lysotracker and QDs.[41] To achieve individual visualization of lysotracker, Hoechst, DyLight™-550 and QDs, different filter cubes were utilized. A filter cube for the QDs was assembled with a rhodamine excitation filter to avoid excitation of lysotracker and a rhodamine emission filter at ~610-630 nm to capture the QDs.

CHAPTER 3: RESULTS AND CONCLUSIONS

3.1 CdSe QD Core Synthesis

The QD CdSe core synthesis produced core sizes ranging from 2-7 nm (calculated using absorption spectroscopy) depending on the reaction duration. Samples were taken in 2 min intervals to determine ideal reaction time to synthesize cores with an emission peak of ~655 nm. Emission at 655 nm does not overlap with other fluorescent dyes used in these microscopy experiments, making this size of QD ideal for co-localization analysis. Above 655 nm (~6 nm diameter) QDs have been shown to lose spherical morphology, becoming more rod-like[1]. Because calculations used to coat the cores with ZnS are based on QDs with spherical morphologies, larger QDs with rod-like morphologies were avoided. CdSe cores quickly grow to red-emitting QDs over the course of only a few minutes (Figure 3.1, 3.2). While core growth was consistent, some delay in core growth was observed over time as the amount of Cd and Se precursor diminished. This could be adjusted by increasing temperature, or precursor solution concentrations, to increase or decrease QD diameter, making each synthesis tunable to obtain the desired size. Early trials were successful, but as the reaction conditions and setup was optimized, QD products demonstrated an increase in fluorescence intensity. While the first successful QD core products had a relative fluorescence unit (RFU) value of only ~600 RFU, more recent trials have obtained values of ~27,000 RFU. While the degree of fluorescence intensity is relative to each synthesis, visual inspection confirmed the significant increase fluorescent intensity with optimized conditions. The quality of each synthesis was further improved with an adjustment of solvent from pure octadecene

to a 50:50 mixture of octadecene:oleylamine. This mix was found to act as a better coordinating ligand to improve the size monodispersity of each synthesis. The mixture also allowed for higher temperatures to be stably maintained, raising the maximum stable temperature from ~280°C to over 300°C. This reduced the amount of time necessary to obtain quality red-emitting QDs from ~45 min to ~20 min. The solvent switch resulted in much more consistent growth rates of QD cores, and a higher quality CdSe core when viewed under the fluorescence microscope.

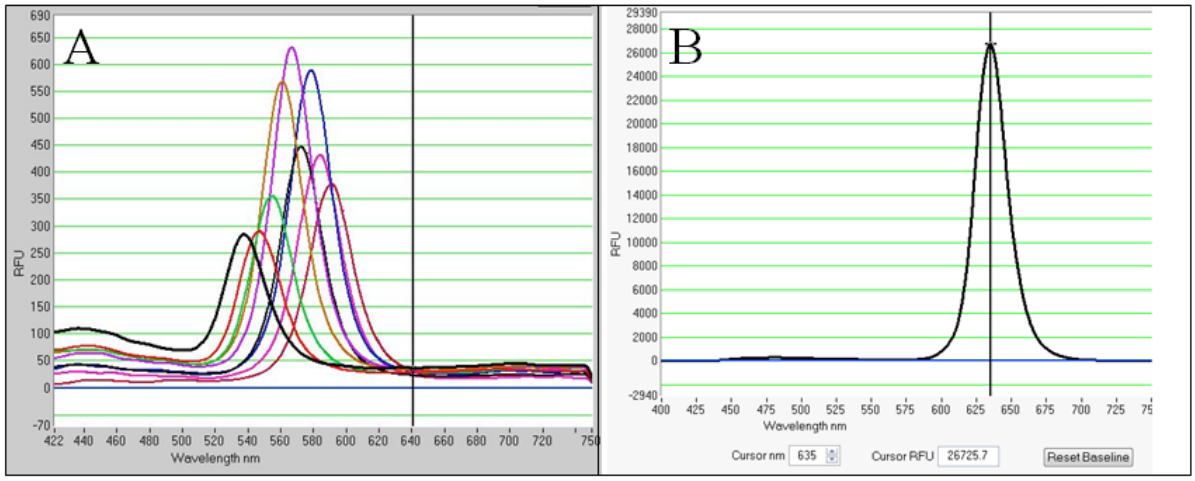

Figure 3.1. Core CdSe Growth Monitored by Fluorescence Spectroscopy. Samples were collected from the reaction mixture every minute to observe core growth rates (A). It was found that reaction for 15 minutes at a temperature of 300°C obtained CdSe QD products with a fluorescence emission of ~630 nm, with a very narrow peak width of ~30 nm (B).

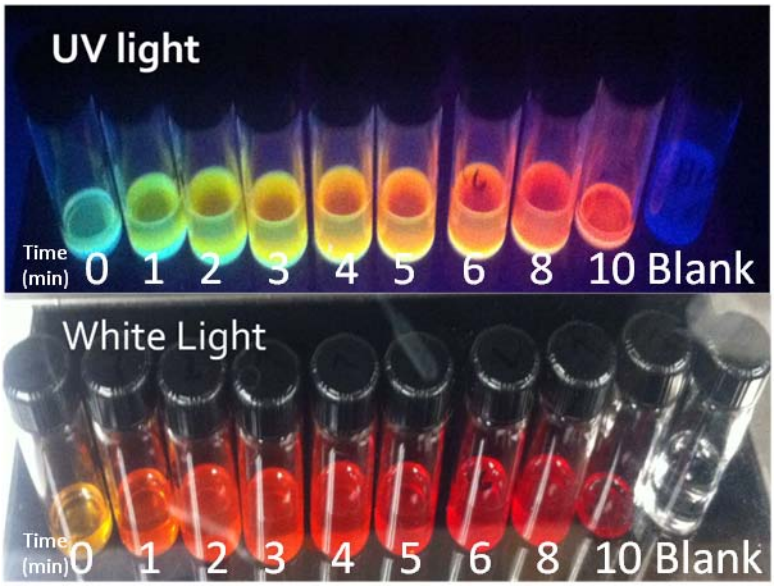

Figure 3.2. Visual Observation of CdSe QD Core Growth. Samples were taken immediately after injection and every minute after to visualize QD growth over time.

Once CdSe cores were synthesized and washed to remove excess precursor, products were experimentally stored in various solvents for 1 week to investigate the effects of solvent on QD fluorescence stability. It was found that hexane was the best solvent for longer storage to reduce quenching. Therefore, CdSe QD cores were stored in hexanes and sealed under nitrogen in a -20°C freezer until subsequent addition of ZnS coating. Storage concentration below 500 nM resulted in increased aggregation (empirical observation). CdSe cores concentrations were calculated to be between 1-4 μM after initial washing steps for most trials.

These highly fluorescent CdSe cores were visualized by a fluorescence microscope and demonstrated distinctive blinking pattern associated with single CdSe QDs. However, visualization with prolonged exposure to UV light demonstrated a blue-shift in fluorescence (from red-orange to yellow, then green) (Figure 3.3). This change in color is speculated to be due to the decrease in QD size as a result of degradation.

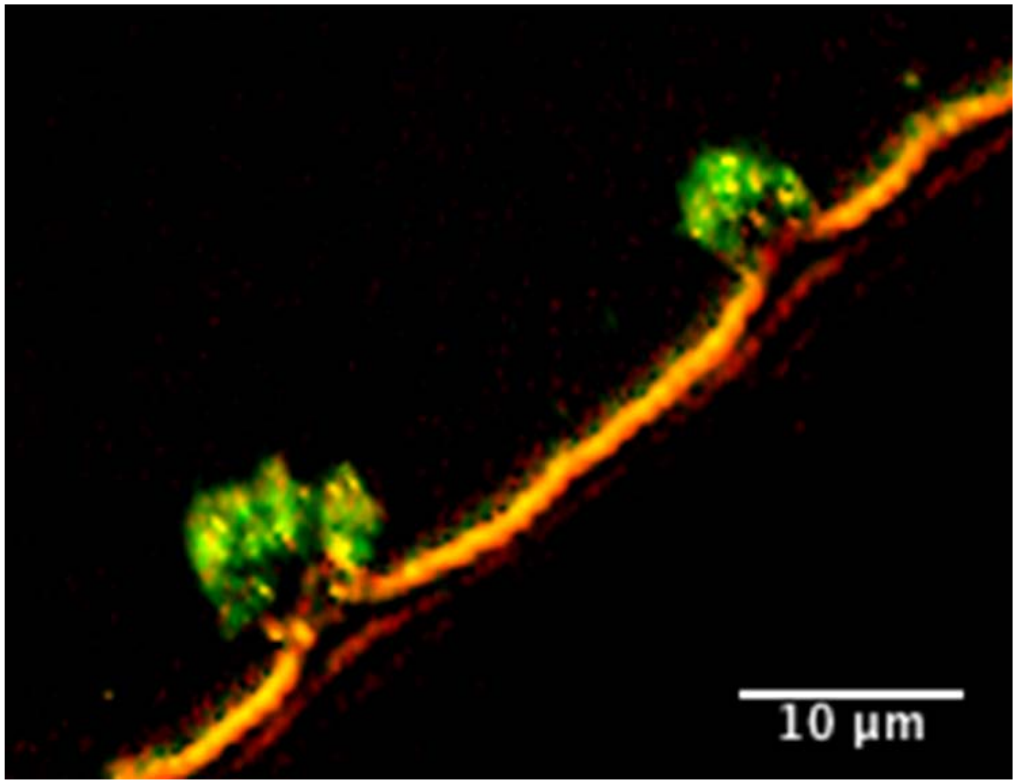

Figure 3.3. CdSe Cores after Prolonged Exposure to UV Light Observed via Fluoresence Microscopy. Orange-red Emitting QDs slowly degrade to emit yellow and green fluorescence after exposure to UV light (~10min). This is a sign of oxidation of the core. The degradation can be controlled with a protective coating on the outside of the cores, both to prevent degradation and correct any imperfections that cause trap states.

The narrow fluorescence emission peak width, indicating monodispersity of QDs, ranged between 26-30 nm at FWHM for a typical synthesis (Figure 3.1). This narrow range indicates that QDs were very monodisperse in size when compared to the theoretical limit for CdSe of 25 nm[42]. QDs that were more monodisperse in size generated core/shell QDs with a more uniform coating (vs. polydisperse CdSe cores) when coated using the SILAR method.

3.2 Passivation of CdSe QDs with ZnS Shells

Addition of a ZnS shell to the outer layer of CdSe cores protects cores from oxidation and degradation. This allows for increased photostability and potentially reduces the toxicity of QDs in biological systems (due to the generation of Cd^{+2} ions during core degradation). Three different methods of ZnS coating were attempted before the SILAR method was selected. The first method attempted was a pyrophoric synthesis with the use of diethyl zinc, an extremely explosive chemical when in contact with air. This method involved injections similar to the SILAR method mentioned in the experimental section, but was much more dangerous. Ultimately, this method was abandoned due to difficulty keeping the reaction in an inert environment during synthesis. The second method (the "sonication method") involved adding zincethylxanthate or zinc stearate in excess and sonicating the mixture at lower temperatures (<80˚C). This method was much easier and required very little setup, but the results of each coating were extremely inconsistent. Many of the CdSe/ZnS products obtained through this method aggregated very quickly compared to the SILAR method (Figure 3.4).

The method that showed the most promise and consistent results was the SILAR method. This method showed immediate improvement of CdSe properties when compared to sonication and pyrophoric methods in both fluorescence intensity and decreased aggregation. More importantly, the SILAR method produced consistent results across trials, coating each CdSe core with 3-5 monolayers (MLs) of ZnS. Successful coatings were evaluated by fluorescence spectra of the QDs and analysis of emission peaks for the characteristic red-shift in λ_{max} of ~5-10 nm. This shift, as well as an increase

in fluorescence intensity, is strong indications of successful ZnS coating (Figure 3.5). ZnS coating was also confirmed using a fluorescence microscope to visualize QDs over the course of ~ 45 minutes with constant UV exposure. QDs visualized this way showed no visual loss of fluorescent intensity or change in fluorescence color.

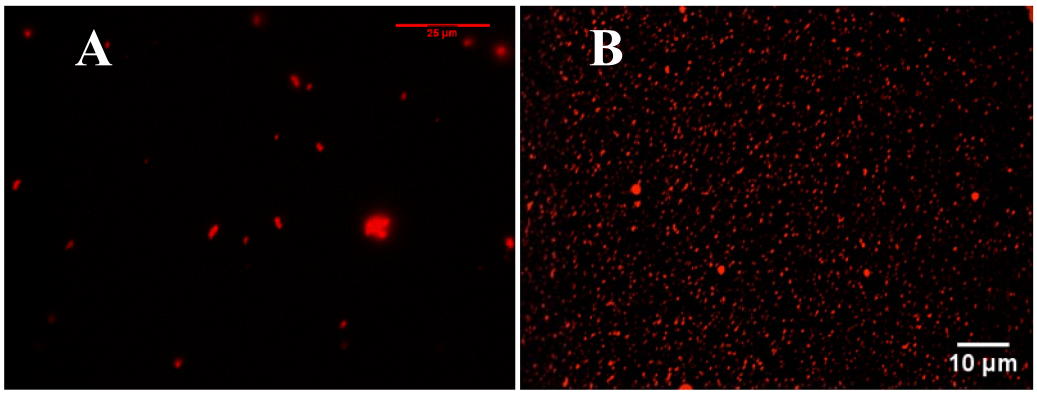

Figure 3.4. Fluorescence Micrographs of CdSe/ZnS QD Products. Aggregation of QDs is easily seen in the sonication method (A). The SILAR method (B), produced much fewer aggregates and demonstrated rapid blinking indicative of single QDs.

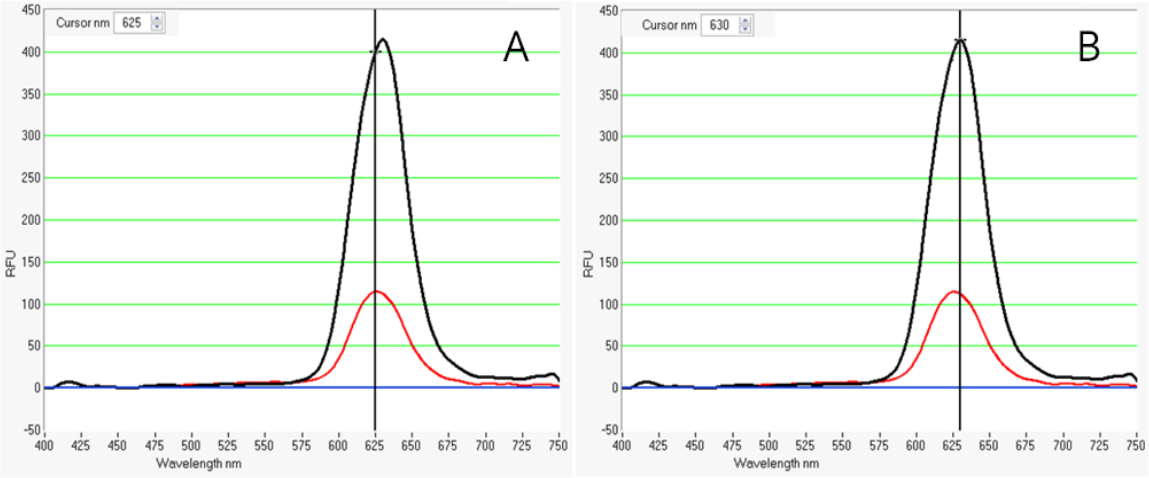

Figure 3.5. Fluorescence Spectrum Characteristics of CdSe vs. CdSe/ZnS QDs. Uncoated CdSe QD cores (Red line) had a maximum emission at ~625 nm (A), while after the same trial of CdSe was coated with ZnS the emission shifted to ~630 nm (B). The λ_{max} of CdSe cores is indicated in A, and λ_{max} of CdSe/ZnS core/shells is indicated in B. The characteristic increase in emission wavelength, as well as an increased intensity from ~110 RFU (red line) to ~410 RFU (black line) is characteristic of successful ZnS shell addition.

3.3 Imparting Water Solubility to CdSe/ZnS QDs

Transferring CdSe/ZnS QDs from organic solvent to water proved to be the single most difficult task in this work. Using an amphiphilic polymer to impart water solubility to the QDs was successful, but suffered from very inconsistent results between trials. Many trials using the amphiphilic polymer resulted in the aggregation of QDs and subsequent precipitation as soon as the THF was completely evaporated. The original polymer used was ~40% diethylamine-modified poly(acrylate) synthesized in-house. However, purification and characterization of this polymer proved laborious and time consuming. Therefore, a commercial polymer, PMAL-d, was used for future trials. A 2,000:1 stoichiometric ratio of polymer:QD was used to ensure excess polymer in solution. Trials using minimal amounts of polymer resulted in precipitation of QD products during centrifugation (~5,000 x g). The stoichiometric ratio of PMAL-d was optimized to ~2,000x molar ratio of CdSe/ZnS QDs for consistent stability in water. Exceeding this ratio resulted in a very turbid solution, likely due to micelle formation. Decreasing this ratio resulted in decreased stability in water (aggregation and precipitation).

While coating QDs with the amphiphilic polymer coatings consistently stabilized QDs into water, there was also a high variance between trials. Many of the QDs aggregated very quickly over the course of ~48 hours. Once out of solution, sonication (that would stabilize CdSe/ZnS cores in organic solvents) only disrupted the polymer coating further, resulting in increased precipitation. The calculated concentration of QDs in solution at this point became invalid; therefore, many trials could not be used for

conjugation steps after this point. QDs that were successfully stabilized in water were visualized on a microscope before use in conjugation trials to ensure consistent long-term stability. Many trials were observed over the course of months with little to no decrease in stability. However, other trials were stable for only 2-3 days before producing a visible precipitate when centrifuged (~5,000 x g). The best trials were observed to be stable for over 6 months in 0.1M borate buffer.

3.4 Surface Modification of Water-Soluble CdSe/ZnS QDs

Once CdSe/ZnS QDs were stable in water, the amphiphilic polymer was functionalized to 1) reduce non-specific interactions with cells, and 2) allow QDs to bind DNA. To reduce non-specific binding of cellular proteins, cPEG and mPEG were conjugated to PMAL-d. This was shown in previous work to reduce non-specific binding of QD nanocarriers in cells[43]. To condense DNA onto QDs, 3-dimethylamino-1-propylamine (DMAPA) was reacted with PMAL-d to increase the net positive surface charge. This increase in charge was intended to allow an electrostatic interaction between QDs and negatively-charged DNA. The amount of positive charge was adjusted by increasing the molar amount of DMTMM used to activate carboxyl groups of the polymer. The increased positive charge allowed for more DNA to electrostatically interact with the surface, causing an increased carrying capacity of the QD for DNA. These two reactions were performed sequentially (first PEGylation, and then reaction with DMAPA) in preliminary experiments. A positive charge of ~+30 mV (Table 3.1) is indicative of successful tertiary amine functionalization. These were compared with standard values of unfunctionalized QDs (-10 to -30 mV)[44] and can be seen below:

Sample	Zeta Potential (mV)
15 nM Water Soluble QD-PEG/*tert*-amine-1	28.94
15 nM Water Soluble QD-PEG/*tert*-amine QDs-2	31.60
15 nM Water Soluble QD-PEG/*tert*-amine QDs-3	29.10
15 nM Water Soluble QD-PEG/*tert*-amine QDs -4	32.00
15 nM Water Soluble QD-PEG/*tert*-amine QDs-5	30.12
Mean	30.35
Std Dev	1.40
Std Error	0.63
Water Soluble CdSe QDs (unfunctionalized)	(-10) to (-30)[44]

The zeta potential values of ~30 mV suggest an electrostatic interaction between DNA and the conjugated QD-PEG/*tert*-amine is possible, via the net positive charge of the conjugated QD and anionic DNA species. The stoichiometric ratio of DMAPA was increased as much as possible in an attempt to increase the charge, but large increases caused loss of stability and aggregation. To investigate the ability of positively functionalized CdSe/ZnS QDs to bind DNA, the plasmid pEGFP-Rab5 was used.

3.5 Plasmid DNA Replication and Characterization

The plasmid DNA used in this work was pGFP-EEA1 purchased from Addgene, which encodes for an early endosomal marker fused to GFP. Because cells successfully transfected with pGFP-EEA1 are expected to express visible green fluorescence (early endosomes), this plasmid was used as a reporter gene in lieu of therapeutic DNA. This allowed for an easy confirmation of successful transfection. Stock pDNA was purified from *E. coli* (described in Chapter 2), then confirmed by digestion with restriction endonucleases *XbaI*, and a combination of *XhoiI* and *EcorRI*. These endonucleases cleave

the DNA at specific sites into fragments with a known size. The resulting fragments were then characterized via electrophoresis (Figure 3.6). The size of the fragments in each band was estimated using a standard DNA ladder, indicating the plasmid from adgene replicated was the correct plasmid predicted.

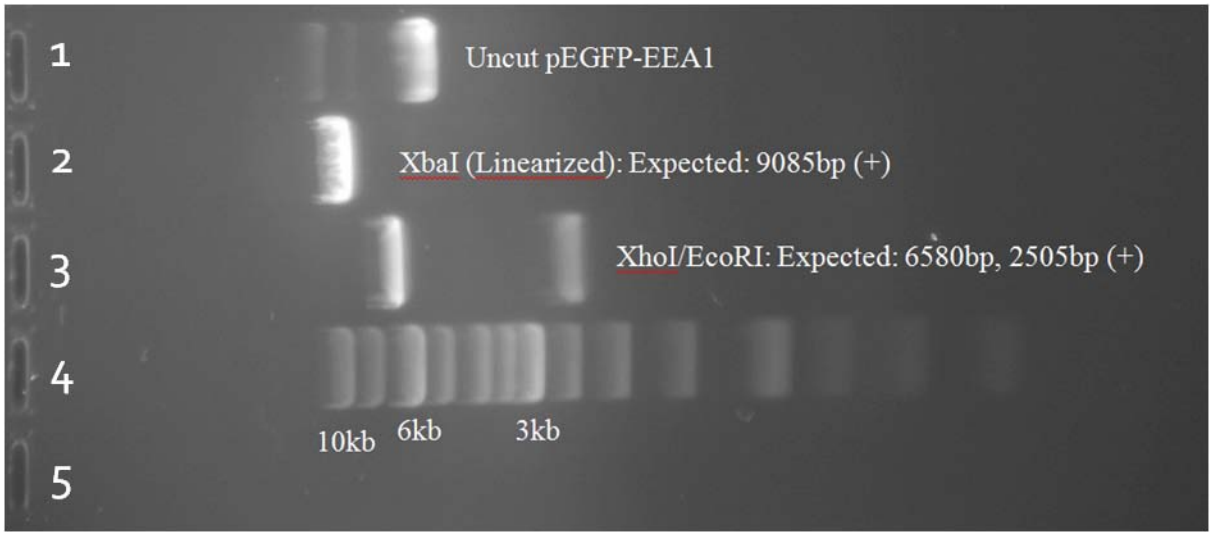

Figure 3.6. Electrophoretic Analysis of pDNA after Restriction Endonuclease Digestion. pGFP-EEA1 was digested in 2 ways: with XbaI to linearize the plasmid (9,085 base pairs), double digestion with XhoI and EcoRI to cut the plasmid into 2 bands produced 2 fragments (6,580 and 2,505 base pairs). The uncut plasmid can also be seen in the top lane in the linear, knicked and supercoiled (left to right) pattern of uncut plasmids.

3.6 Characterization of pDNA and QD-Conjugate Interactions

The interactions of pDNA with QD-PEG/*tert*-amine was evaluated through electrophoretic gel-shift assay to investigate the ability of QD conjugates to complex pDNA (i.e. slower gel migration rates vs. uncomplexed pDNA). Preliminary evaluation confirmed the presence of pDNA interaction with conjugated QDs. QDs and pDNA were added together to incubate at RT for ~30 mins before being loaded into each well. For this trial, an excess of QDs was combined with a low molar amount of pDNA that could

be visualized with SYBR green (detection limit ~1-2 ng[45]). The result seen in Figure 3.7, Comparing the ability of in-house synthesized QDs and commercial QDs to bind pDNA showed that QDs made in-house interacted with DNA, holding DNA within the well of the gel (Figure 3.7). While similarly functionalized commercial QDs were not able to complex pDNA.

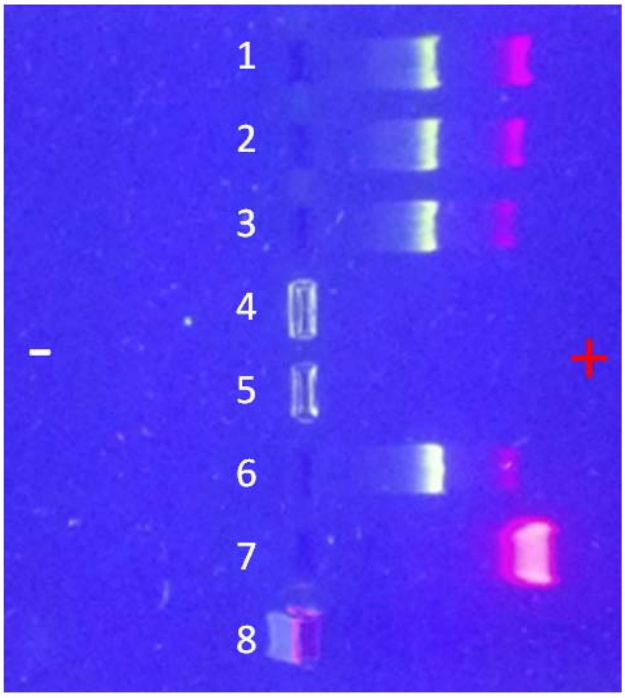

Figure 3.7. Interaction of pDNA with QD-*tert*-amine. Lane 1-3: 1-~50 ng, 2-~100 ng, 3-~500 ng pDNA incubated for 30 mins with 10 µL of 250 nM commercial QDs functionalized with DMAPA, Lane 4,5: 10 µL of 250 nM in-house synthesized QD-PEG/*tert*-Amine was incubated with with 50 ng or, 100 ng pDNA, Lane 6: pDNA alone (some bleedover from commercial QD in Lane 7), Lane 7: Commercial QDs functionalized with DMAPA, Lane 8: In-house QD-*tert*-amine. This gel shows pDNA is retained within the well when incubated with in-house QD-*tert*-amine, but not when incubated with commercial QDs functionalized with DMAPA. QDs (red); pDNA (green).

The electrophoretic gel-shift assay demonstrated that commercial QDs had little-to-no electrostatic attraction to pDNA, even after functionalization with DMAPA to increase net positive charge. This may have been caused by interactions with surface moieties; however, we are unable to fully evaluate the interactions due to the proprietary

nature of the commercial QDs (the identity of water-solubilizing coating of the commercial QDs are not available). DNA-QD complexation was successful in early trials with in-house QDs (Figure 3.7). In-house QDs retained the pDNA within the gel wells. Further trials were performed to optimize this interaction and attempt to complex an average of one pDNA on the surface of each QD. Future work with commercial QDs was abandoned at this point since they did not appear to complex pDNA.

Figure 3.8, demonstrates the effect of increasing the amount of activator in the QD-diamine conjugation in an attempt to increase the net positive charge on QD-*tert*-amine conjguates. Preliminary experiments bound DNA, but did not indicate the limit of how much pDNA could be bound (Figure 3.8A, 150,000 mole DMTMM: 1 mole QD) due to the DNA being retained in all trials. Later experiments demonstrated increased pDNA:QD interaction with increasing diamine functionalization. By increasing the DMTMM ratio, more carboxyl groups could be activated and more positive charge could be imparted onto the QDs. This increae in charge could lead to increased condensation of pDNA onto each QD. At a DMTMM ratio of 375,000 DMTMM:QD the conjugation was able to bind a 1:1 molar ratio of QD:pDNA. Figure 3.8 establishes two main things: 1) the ~1:1 molar ratio pDNA:QD was possible and successful with a 375,000:1 DMTMM:QD excess (C,lane 3), and 2) too much DMTMM, unexpectedly, was unable to increase the binding ability of DNA. This decrease in binding efficency with increase DMTMM may be due to the reaction mechanism reaching a limit to the amount of carboxly groups that can be stably activated in a single reaction. By activating too many with the intermediate, it may decrease the overall water solubility of the compound,

resulting in a preciptate obsreved with increased DMTMM (500,000:1 mol DMTMM:mol QD).

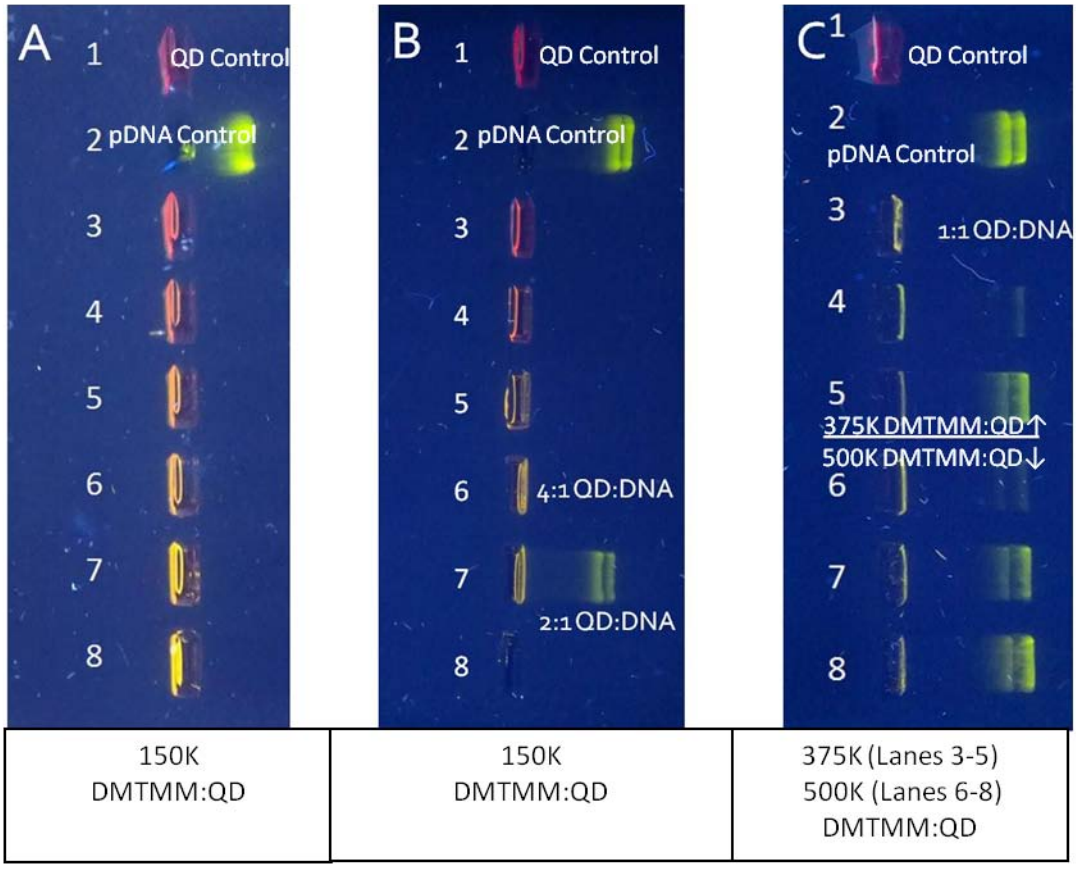

Figure 3.8. Gel-Shift Assays of QD-pDNA complexation. QD was conjugated to DMAPA using increasing amounts of activator (DMTMM) in an attempt to increase the overall positive charge of each QD-*tert*-amine conjugate. Each QD conjugate was incubated with ~10 ng of pDNA (green) for 30 min. In all trials, 10 ng of DNA was used and the amount of QD-*tert*-amine was decreased. In A, QD:DNA molar ratios were higher than needed, indicating we could lower the mol QD used in each trial. For B the QD reached the maximum capacity it could hold with a 2:1 mols QD: mols pDNA. In an attempt to increase this, higher DMTMM concentrations were used until a 1:1 mol ratio of pDNA:QD was attained in lane 3, C.

The fluorescence intensity of QD-PEG/*tert*-amine dropped significantly vs. unfunctionalized QDs, which appeared to be correlated with repeated activation using

DMTMM in each step. To prevent this, functionalization with PEG and DMAPA was performed simultaneously to reduce the exposure of QDs to DMTMM. The successful reaction of QDs with both PEG and DMAPA was confirmed to bind the same amount of DNA as QDs produced in the 2-step reaction.

3.7 Functionalization of Diamine/PEG QDs to Wheat Germ Agglutinin

With QD-PEG/*tert*-amine binding pDNA effectively at a 1:1 molar ratio the next conjugation was to biofunctionalize QDs with WGA. Wheat germ agglutinin (WGA) has been previously shown to bind to the nuclear membrane of the cell[46], which is why it was chosen for this work. WGA is a sugar-binding protein (lectin) that our lab suspects could aid the trafficking of QD vectors through early endosomes, into the Golgi apparatus, through the endoplasmic reticulum and, potentially, into the nucleus. To exploit this pathway, WGA was conjugated to maleimide-activated QD-PEG/*tert*-amine at a ~1:1 ratio (1WGA:1QD-PEG/*tert*-amine). To conjugate WGA to the QD-PEG/*tert*-amine two steps were required 1) maleimide was conjugated to the QD-PEG/*tert*-amine (Figure 2.3) and 2) a maleimide reaction with the free sulfhydryl in cysteine groups on WGA. There are 4 free sulfhydryl groups within WGA. These groups are located close together in both subunits of WGA. Stoichiometry was closely monitored to prevent aggregation of multivalent products. If the QD were to react with one of these groups, steric hindrance is expected to hinder reaction with a second free sulfhydryl, decreasing the likelihood of a multivalent product. However, a second attachment of WGA is still possible.

Confirmation of WGA conjugation proved challenging, and ultimately unsuccessful. Confirmation of WGA to the QD-PEG/*tert*-Amine QD conjugate was

attempted using a protein assay (fluorescamine assay). However, PMAL-d on the QD surface exhibited high background, decreasing the sensitivity of this method. Circular dichroism (CD) spectroscopy was also used to verify the presence of secondary structures in WGA. Being mostly alpha helices, WGA alone exhibited the expected characteristic peak dip signal (Figure 3.9). While the expected spectral characteristics were present, the WGA concentration of purchased WGA was much higher (13 µM to 130 nM) than our QD-WGA conjugates (10-15 nM or lower). This method was not sensitive enough to obtain reliable spectra at these concentrations, and performing larger scale reactions at this time was not feasible due to time constraints.

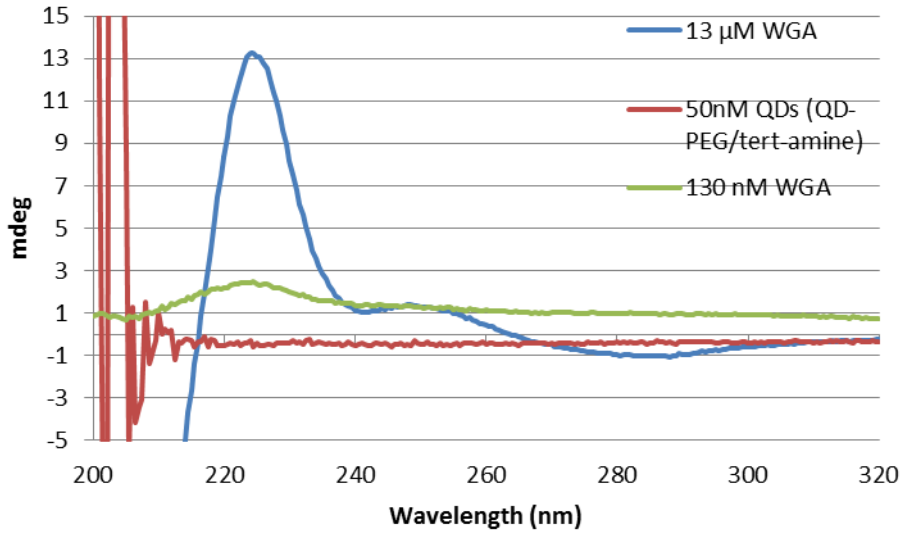

Figure 3.9. Circular Dichroism Spectroscopy of WGA. WGA and QDs were evaluated on a CD spectraphotometer to determine if the technique could be used to test for presence or absence of WGA on QD conjugates. While QD-PEG/tert-amine showed little more than a baseline signal. The WGA signal was almost undectectable at 130 nM concentrations, 10x the theoretical amount in our WGA-QD conjugates.

3.8 Intracellular Tracking of WGA-QD Conjugates

The next step was to treat cells with QD-WGA conjugates to investigate intracellular trafficking. Initial incubations with QD-WGA conjugates were used to give a preliminary indication of cellular internalization (Figure 3.10). QD-WGA conjugates were incubated with a 1:1 molar ratio pDNA for 30 min before incubation with HeLa cells for 4 hours. After 4 hours, the cells were fixed and treated with fluorescent Hoechst dye (nuclear label). The QDs were internalized and localized around the nucleus (Figure 3.10). However it is inconclusive if cellular location was from QDs exploiting the proposed pathway (EE→Golgi→ER→nucleus) or if QDs localized within lysosomes, which are also perinuclear. Additional experiments to investigate cellular localization were needed. These trials were performed with and without the presence of pDNA complexed to the QD surface, but the addition of pDNA had little-to-no effect.

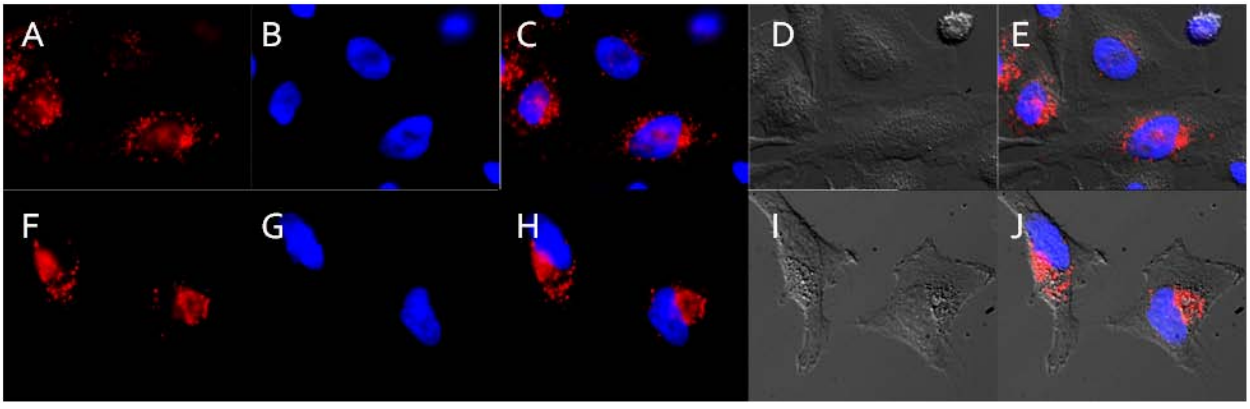

Figure 3.10. Internalization of WGA-QD Complexes with HeLa Cells.1:1 mol QD:mol WGA (A-E), 1:5 mol QD:mol WGA (F-J) . HeLa cells were incubated with QD-WGA complexes (red) for 4 hours and counterstained with Hoeschst (blue). These trials demonstrated the intracellular location of QD-WGA complexes. There was little to no difference in the amount of WGA (1:1 or 1:5) incubated with HeLa. The QDs (A,F) were overlaid with Hoeschst dye (B,G) to create a combination of only fluorescence (C,H) before being combined with differential interference contrast images (DIC, D,I) to give a full representation of the cell (E,J).

The aforementioned intracellular trafficking experiment was repeated with the QD-WGA conjugates using Immunocytochemistry (ICC) to label the Golgi apparatus. Analysis of these images revealed little colocalization between the Golgi apparatus and QD-WGA (Figure 3.11). Images were subjected to Manders' colocalization analysis, which returned an M_{QD} value (red pixels overlapping green pixels) of only 0.327. The smaller value agreed with this initial view of little colocalization, indicating many QDs were not in the Golgi apparatus.

Experiments to investigate co-localization with lysosomes indicated high localization with the lysosome (Figure 3.12). While this is positive results of QDs localization within the cell, it showed that the QDs were likely not following the proposed pathway through the Golgi apparatus, but being degraded by lysosomes. The degree of overlap between the Golgi apparatus:QD and Lysosome:QD was 0.327 and 0.903 respectively. Unfortunately, was not a significant overlap between QD-WGA conjugates and the Golgi apparatus, which indicates that WGA conjugation was likely unsuccessful.

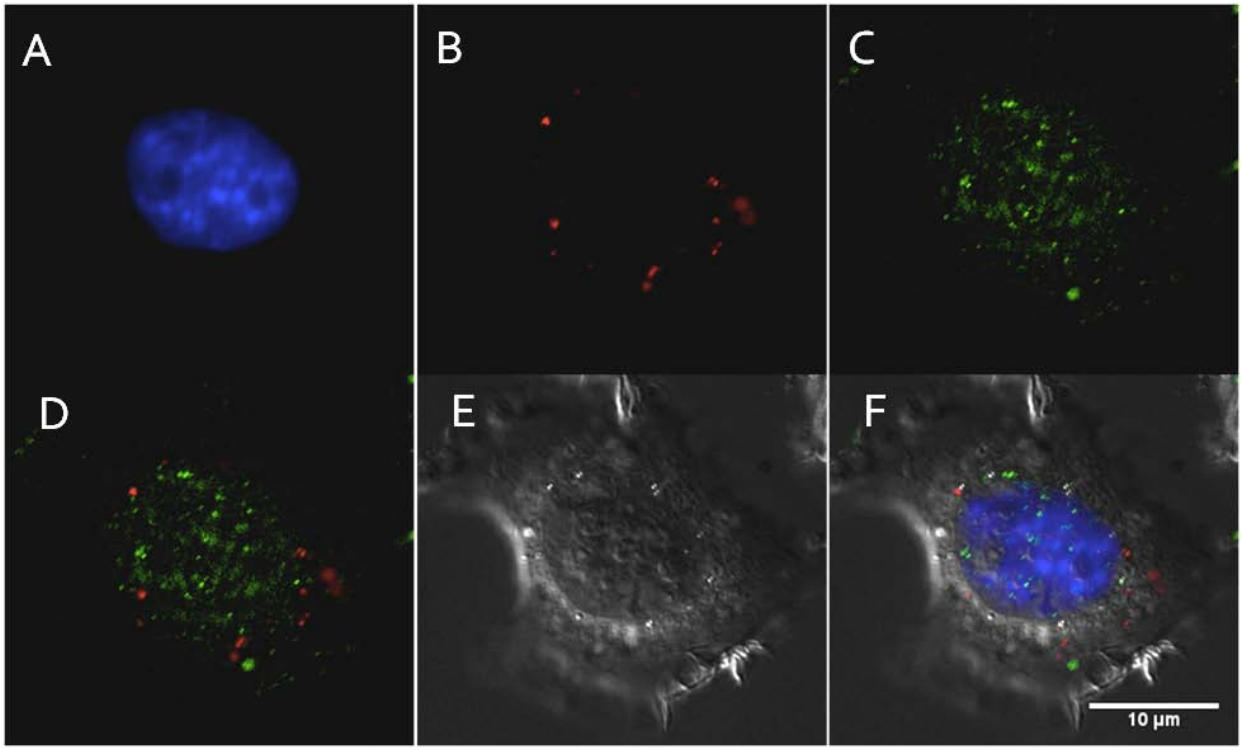

Figure 3.11. Co-localization of QD-WGA Complexes with the Golgi Apparatus. N2A cells were labeled with Hoechst (A), QDs (B) and a Golgi marker (C) then visualized with an overlay of the QDs and Golgi marker (D), DIC image of the cells (E) and a compilation of all 4 images (F).

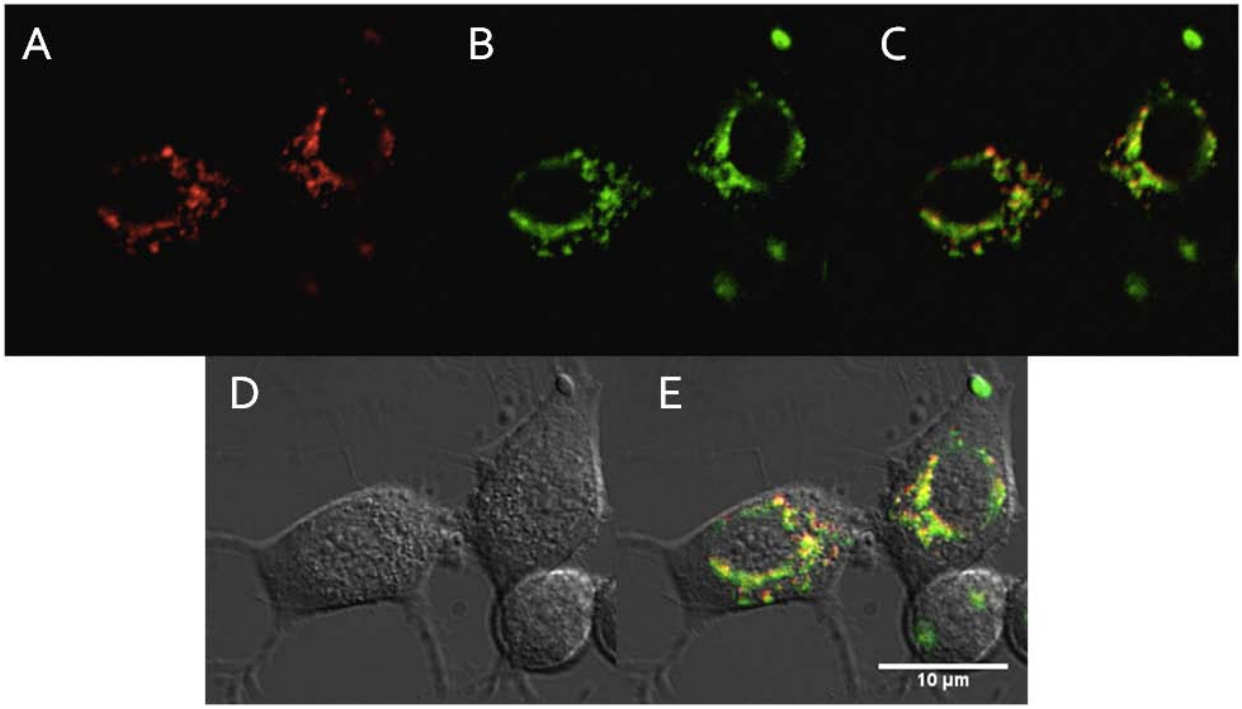

Figure 3.12. Co-localization of QD-WGA Conjugates with Lysosomes in N2a Cells. QDs (A) and Lysotracker (B)were overlaid (C) and combined with a DIC image of the cells (D) to create a full view of the cell. Lysosomal marker (lysotracker) co-localized within the cell to a high degree, visualized as yellow when red is overlaid with green.

3.9 Conclusions and Future Works

This project explored the ability to use bioconjugated WGA-QDs as non-viral gene therapy vectors. Although additional information is required to determine if WGA can be used as a nuclear targeting agent for DNA delivery, these initial attempts have demonstrated the optimization of CdSe QD synthesis; successful ZnS coating for higher quality, photostable QDs; successful water solubilization techniques; functionalization of QDs to increase DNA binding, and carefully considered conjugation schemes. WGA conjugation was performed, but more careful analysis to confirm WGA conjugation is necessary. Preliminary intracellular trafficking experiments have been completed, but additional characterization is necessary for conclusive discussion as to if the localization

to the lysosome was intrinsic in QD-WGA conjugates or if it was due to a lack of WGA conjugation.

Many more studies can be done to increase the endocytic selectivity and stability of these QDs for gene therapy applications. Herein, our lab has demonstrated that the quality CdSe QDs cores were increased with each trial. The successive ionic layer adsorption and reaction (SILAR) method demonstrated an increase of fluorescence and slight increase in maximum fluorescence emission peak. The largest hurdle in this work was water solubilization of the synthesized QDs. This step took much longer than anticipated, and even when successful the amphiphilic polymer method did not produce QDs with consistent water solubility. Other ligands or amphiphilic polymers can be used to optimize the water solubilization of these QDs. Current work focuses on possible water solubilization through the use of bidentate ligand exchange methods in place of amphiphilic polymer coatings. While later trials of QD-WGA conjugation resulted in possible lysosomal degradation, it may have been due to the instability of the polymer causing issues when reacted in subsequent conjugations, causing many trials to precipitate out of solution. The stability of the QDs in water is the prime concern for conjugation validity. Current work is focused on developing more stable water-soluble QDs using functionalized lipoic acid as a ligand reagent.

A second major concern is the degradation of Cd-based QDs in live cells. Trafficking of these Cd-based QDs to the acidic environment of the lysosomes could result in the degradation of the metallic nanocrystals, leading to the release of Cd^{+2} ions, which are toxic. The use of CdSe QDs, while being the most popular QD composition in biomedical research, has many alternatives. Indium is one of the more common

alternatives that maintains a high degree of fluorescence intensity without the use of cadmium, mitigating toxicity. Current work is underway to investigate indium-based core synthesis.

References

1. Anderson, K. E., Fong, C. Y. & Pickett, W. E., Quantum Confinement in CdSe Nanocrystallites. *Journal of Non-Crystalline Solids*, **299-302** 1105-1110 (2002).

2. Michalet, X. et al., Quantum Dots for Live Cells, in Vivo Imaging, and Diagnostics. *Science Magazine*, **307** 538-544 (2008).

3. Allen, P. M., Semiconductor Nanocrystals: Synthesis, Mechanisms of Formation, and Applications in Biology (Thesis, Massachusetts Institute of Technology, 2006).

4. Fichter, K. M., Flajolet, M., Greengard, P. & Vu, T. Q., Kinetics of G-Protein-Coupled Receptor Endosomal Trafficking Pathways Revealed by Single Quantum Dots. *PNAS*, **107** 18658-18663 (2010).

5. Angell, J. J., Synthesis and Characterization of CdSe-ZnS Core-Shell Quantum Dots for Increased Quantum Yield (Thesis, California Polytechnic State University, San Luis Obispo, 2011).

6. Sigma Aldrich, Quantum Dots, Available at http://www.sigmaaldrich.com/materials-science/nanomaterials/quantum-dots.html (2015).

7. Torchynska, T. & Vorobiev, Y., in *Advanced Biomedical Engineering*, edited by Gargiulo, G. D. (InTech, 2011), pp. 143-183.

8. Yu, W. W., Qu, L., Guo, W. & Peng, X., Experimental Determination of the Extinction Coefficient of CdTe, CdSe, and CdS Nanocrystals. *Chem. Mater.* **15** (14), 2854-2860 (2003).

9. Vetter, T., Iggland, M., Ochsenbein, D., Hanseler, F. & Mazzotti, M., Modeling Nucleation, Growth, and Ostwald Ripening in Crystalization Processes: A Comparison between Population Balance and Kinetic Rate Equation. *Crystal Growth and Design*, **13** (11) 4890-4905 (2013).

10. Bawendi, M. G., (CdSe)ZnS Core-Shell Quantum Dots: Synthesis and Characterization of a Size Series of Highly Luminescent Nanocrystallites. *J. Phys. Chem.* B**, 101** (46), 9463-9475 (1997).

11. Dickerson, B., Organometallic Synthesis Kinetics of CdSe Quantum Dots (Virginia Polytechnic Institute and Sate University, Blacksburg, 2005).

12. Thompson, K. F., Modification of Polymeric Substrates using Surface-Grafted Nanoscaffolds (Georgia Institute of Technology, 2005), Vol. Dissertation.

13. Hines, D. A., Becker, M. A. & Kamat, P. V., Photoinduced Surface Oxidation and Its Effect on the Exciton Dynamics of CdSe Quantum Dots. *The Journals of Physical Chemistry* **116** (24), 13452-13457 (2012).

14. Yu, W. W., Chang, E., Drezek, R. & Colvin, V. L., Water-Soluble Quantum Dots for Biomedical Applications. *Biochemical and Biophysical Research Communications,* **348** (3), 781-786 (2006).

15. Tsol, K. M., Dai, Q., Alman, B. A. & Chan, W. C. W., Are Quantum Dots Toxic? Exploring the Discrepancy Between Cell Culture and Animal Studies. *Accounts of Chemical Research* **46** (3), 662-667 (2013).

16. Alivisatos, P. A., Gu, W. & Larabell, C., Quantum Dots as Cellular Probes. *Annual Review of Biomedical Engineering*, **7** 55-76 (2005).

17. Janczewski, D., Tomczak, N., Han, M.-Y. & Vancso, G. J., Synthesis of Functionalized Amphiphilic Polymers for Coating Quantum Dots. *Nature Protocols*, **6** 1546-1553 (2011).

18. Cavazzana-Calvo, M., Thrasher, A. & Mavilio, F., The Future of Gene Therapy. *Nature* **427**, 779-781 (2004).

19. Genetic Science Learning Center, Learn.Genetics, Available at http://learn.genetics.utah.edu/content/genetherapy/gttools/.

20. Yi, Y., Jong Noh, M. & Hee Lee, K., Current Advances in Retroviral Gene Therapy. *Current Gene Therapy*, 218-228 (2011).

21. Elouahabi, A. & Ruysschaert, J.-M., Formation of Intracellular Trafficking of Lipoplexes and Polyplexes. *Molecular Therapy* **11** (3), 336-345 (2005).

22. Life Technologies, How Cationic Lipid Mediated Transfection Works, Available at www.lifetechnologies.com/us/en/home/references/gibco-cell-culture-basics/transfection-basics/gene-delivery-technologies/cationic-lipid-mediated-delivery/how-cationic-lipid-mediated-transfection-works.html (2015).

23. Ginn, S. L., Alexander, I. E., Edelstein, M. L. & Abedi, M. R., Gene Therapy Clinical Trials Worldwide to 2012-An Update. *The Journal of Gene Medicine* **15**, 65-77 (2013).

24. Medina, L., Intracellular Trafficking of Nonviral Vectors. *Gene Therapy*, 1734-1751 (2005).

25. Alberts, B. et al., *Molecular Biology of the Cell*, 4th ed. (Garland Science, New York, 2002).

26. Rejman, J., Bragonzi, A. & Conese, M., Role of Clathrin- and Caveolae-Mediated Endocytosis in Gene Transfer Mediated by Lipo- and Polyplexes. *Molecular Therapy*, 468-474 (2005).

27. Bentzen, E. L., Tomlinson, I. D., Mason, J. & Gresch, P., Surface Modification to Reduce Nonspecific Binding of Quantum Dots in Live Cell Assays. *Bioconjugate Chemistry*, 1488-1494 (2005).

28. Fichter, K. M., Zhang, L., Kiick, K. L. & Reineke, T. M., Peptide-Functionalized Poly(ethylene glycol) Star Polymers: DNA Delivery Vehicles with Multivalent Molecular Architecture. *Bioconjugate Chemistry*, 76-88 (2008).

29. Murcia, M. J. & Naumann, C. A., in *Nanotechnologies for the Life Sciences* (Wiley, Weinheim, 2005), pp. 1-40.

30. Resch-Genger, U., Quantum Dots vs Organic Dyes as Fluorescent Labels. *Nature* **5** (9), 763-775 (2008).

31. Nelson, D. L. & Cox, M. M., *Lehninger Principles of Biochemistry*, 5th ed. (W. H. Freeman and Company, New York, 2008).

32. Burry, R. W., Controls for Immunocytochemistry: An Update. *Journal of Histochemistry and Cytochemistry*, 6-12 (2011).

33. Carl Zeiss Microscopy, in *Microscopy from Carl Zeiss* (BioSciences, Jena, 2014).

34. Olympus, Basics of Inverted Microscope, Available at http://www.olympus-lifescience.com/en/microscopes/inverted/ (2015).

35. Dunn, K. W., Kamocka, M. M. & McDonald, J. H., A Practical Guide to Evaluating Colocalization in Biological Microscopy, Available at http://www.ncbi.nlm.nih.gov/pmc/articles/PMC3074624/ (2011).

36. Protière, M. & Reiss, P., Highly Luminescent Cd1-xZnxSe/ZnS Core/Shell Nanocrystals Emitting in the Blue-Green Spectral Range. *Small* **3** (3), 399-403 (2007).

37. Gao, X. et al., In Vivo Molecular and Cellular Imaging with Quantum Dots. *Analytical Biotechnology* **16**, 63-72 (2005).

38. Sigma Aldrich, Products, Available at www.SigmaAldrich.com/catalog/product/sigma/90771.

39. Adam, S. A., Marr, R. S. & Gerace, L., Nuclear Protein Import in Permeabilized Mammalian Cells Requires Soluble Cytoplasmic Factors. *The Journal of Cell Biology* **111**, 807-816 (1990).

40. Hermanson, G. T.*, Bioconjugate Techniques*, 3rd ed. (Academic Press, Rockford, IL, 2013).

41. Thermo Fisher Scientific, Life Technologies, Available at https://www.lifetechnologies.com/order/catalog/product/L7525.

42. Hai, L. B. et al., in *Physis and Engineering of New Materials*, edited by Cat, D. T. (Springer, 2009), pp. 79-86.

43. Fichter, K. M., Ingle, N. P., McLendon, M. P. & Reineke, T. M., Polymeric Nucleic Acid Vehicles Exploit Active Interorganelle Trafficking Mechanisms. *ACS Nano* **7** (1), 347-364 (2013).

44. STREM, in *STREM Catalog* (STREM, 2010).

45. Sigma Aldrich, in *Sigma Aldrich* (Sigma Aldrich, St. Louis, 2015).

46. Adam, S. A., Marr, R. S. & Gerace, L., Nuclear Protein Import in Permeabilized Mammalian Cells Requires Soluble Cytoplasmic Factors. *The Journal of Cell Biology* **111**, 807-816 (1990).